Bioactive Materials 49 (2025) 362–377

Contents lists available at ScienceDirect

Bioactive Materials

journal homepage: www.keaipublishing.com/en/journals/bioactive-materials

Sequential construction of vascularized and mineralized bone organoids using engineered ECM-DNA-CPO-based bionic matrix for efficient bone regeneration

Tingting Gai [a,b,c,d,e,1], Hao Zhang [a,b,e,f,1], Yan Hu [f,1], Ruiyang Li [f,1], Jian Wang [a,b,e,f], Xiao Chen [f], Jianhua Wang [f], Zhenhua Chen [g], Yingying Jing [a,b,e], Chenglong Wang [g,*], Long Bai [a,b,e,**], Xiuhui Wang [a,b,e,***], Jiacan Su [a,b,e,f,****]

[a] Institute of Translational Medicine, Shanghai University, Shanghai, 200444, China
[b] Organoid Research Center, Shanghai University, Shanghai, 200444, China
[c] School of Medicine, Shanghai University, Shanghai, 200444, China
[d] School of Life Sciences, Shanghai University, Shanghai, 200444, China
[e] National Center for Translational Medicine (Shanghai) SHU Branch, Shanghai University, Shanghai, 200444, China
[f] Department of Orthopedics, Xinhua Hospital, Shanghai Jiao Tong University School of Medicine, Shanghai, 200092, China
[g] Yantai Zhenghai Bio-tech Co., Ltd, Yantai, 264006, China

ARTICLE INFO

Keywords:
Bionic matrix
Bone microenvironment
Mineralization
Vascularization
Bone organoids
Bone regeneration

ABSTRACT

Given the limitations of allogeneic and artificial bone grafts, bone organoids have attracted extensive attention for their physiological properties that closely resemble natural bone, offering great potential to bone reconstruction for critical-sized bone defects. Although early-stage bone organoids such as osteo-callus organoids and woven bone organoids have been reported, functional bone organoids with vascularization and mineralization are currently unavailable due to the lack of bone-mimicking matrix and dynamic culture systems suitable for the long-term cultivation of mature bone organoids. Herein, a novel engineered bionic matrix hydrogels with multifunctional components and double network structure are developed by incorporating calcium phosphate oligomers (CPO) into a combination of bone-derived decellularized extracellular matrix (ECM) and salmon-derived deoxyribonucleic acid (DNA) via photo-crosslinking and dynamic self-assembly strategies. This kind of bionic matrix hydrogels facilitate recruitment, proliferation, osteogenesis and angiogenesis of bone marrow mesenchymal stromal cells (BMSCs). More importantly, vascularized and mineralized bone organoids are sequentially constructed using BMSCs-loaded engineered bionic matrix hydrogels via *in vitro* dynamic culture and *in vivo* heterotopic ossification. Meanwhile, this kind of engineered bionic matrix are capable of achieving efficient bone repair for cranial defect. These findings suggest that engineered bionic matrix hydrogels combined with such dynamic culture system, providing a promising strategy for functional bone organoids construction.

1. Introduction

Bone tissue, as a dynamic load-bearing structure of living organisms, regulates mineral homeostasis, blood-forming, and mechanically protect vital internal organs [1–3]. However, various of bone defects caused by tumor, trauma, infection and age-induced diseases will compromise the integrity of skeleton, further restrict the normal activities of the body [4–6]. The repair of large bone defects remains a major challenge in

Peer review under the responsibility of KeAi Communications Co., Ltd.
* Corresponding authors.
** Corresponding author. Institute of Translational Medicine, Shanghai University, Shanghai, 200444, China.
*** Corresponding authors. Institute of Translational Medicine, Shanghai University, Shanghai, 200444, China.
**** Corresponding author. Institute of Translational Medicine, Shanghai University, Shanghai, 200444, China.
E-mail addresses: wangorth@163.com (C. Wang), bailong@shu.edu.cn (L. Bai), blackrabbit@shu.edu.cn (X. Wang), drsujiacan@163.com (J. Su).
[1] These authors contributed equally to this work.

https://doi.org/10.1016/j.bioactmat.2025.02.033
Received 2 January 2025; Received in revised form 20 February 2025; Accepted 21 February 2025

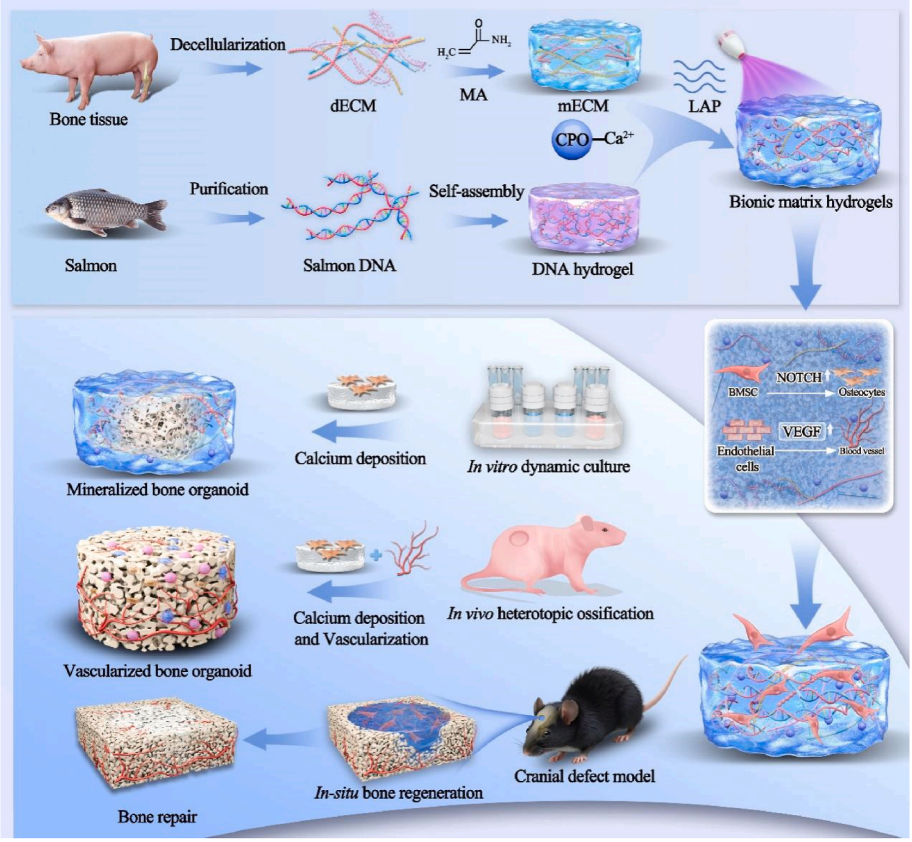

Scheme 1. Schematic diagram of the sequential construction of vascularized and mineralized bone organoids using engineered ECM-DNA-CPO bionic matrix hydrogels that mimicked bone dynamic microenvironment with multifunctional components and double network structure.

clinical orthopedics, primarily because of the limited natural regenerative potential of the body's own cells [7,8]. Considering the drawbacks of existing clinical methods, like autologous and allogeneic bone grafts, which are hindered by a shortage of donors and the risk of immune rejection [9,10], *in vitro* replication of the complex structures and functions of specific bone tissues has become a long pursuit to achieve the reconstruction of bone defects [11–13].

Bone organoids have attracted significant interest in bone tissue repair because their physiological characteristics closely mimic those of natural bone [14–17]. Different from soft tissue organoids via self-assembling from 3D cellular clusters [18–20], bone organoids require a mineralized structure replied on special inorganic/organic hybrid extracellular matrix, which mimic the loading-bearing capacity of natural bone [21–24]. More importantly, bone organoids must be able to respond to biochemical signals in a dynamic environment, supporting the vascularization and other functions [25–27]. These requirements increase the complexity of constructing functional bone organoids. Hofmann et al. firstly reported a kind of woven bone organoids via functional 3D self-assembly of osteoblasts and osteocytes derived from the *in vitro* differentiation of human bone marrow stromal cell (BMSCs), in which mineralized matrix produced by the balance of osteocytes and osteoblasts under biological control [28]. Besides, Ouyang et al. developed a novel type of osteo-callus organoids via endochondral ossification by stepwise-induction *in vitro* using BMSCs-loaded GelMA hydrogel microspheres. This kind of osteo-callus organoids closely resembled the diverse cell compositions and dynamic processes seen in developmental endochondral ossification, enabling rapid bone regeneration in large bone defects [29]. While above-reported bone organoids including osteo-callus organoids and woven bone organoids were still classified as early-stage bone model, functional bone organoids with vascularization and mineralization are currently unavailable due to the lack of bone-mimicking matrix and dynamic culture systems suitable for the long-term cultivation of mature bone organoids.

To create a bionic bone environment for the construction of functional bone organoids, bone-mimicking matrix hydrogels should replicate the natural composition of bone tissue [30–33]. Bone derived decellularized extracellular matrix (dECM) is considered as an ideal material for fully mimicking organic components of the native bone matrix [34–36]. Numerous past studies have demonstrated that bone dECM can enhance the recruitment, proliferation, and differentiation of BMSCs [37,38]. Furthermore, inorganic materials of bone-mimicking matrix represent another crucial component in the bone-mimicking hydrogel substrates. Although hydroxyapatite (HAp) could bind with the extracellular matrix (ECM), its relatively high crystallinity and slow degradation rate hinder the formation of bone organoid formation [39]. Calcium phosphate oligomers (CPO) exhibited proper degradation rate, osteogenic and angiogenic abilities, which could accelerate the mineralization and vascularization of BMSCs within bone-mimicking matrix, further facilitate formation of mineralized bone organoids [40–42]. In addition, deoxyribonucleic acid (DNA) contains abundant phosphate groups, which could enhance interactions with Ca^{2+} ions released from CPO, thereby accelerating mineralization in bone organoid construction [43–45].

Taken together, we developed a novel engineered bionic matrix hydrogels loaded with BMSCs for sequential construction of vascularized and mineralized bone organoids via *in vitro* dynamic culture and *in vivo* heterotopic ossification (Scheme 1). In which, engineered bionic matrix hydrogels are composed of such ECM-DNA-CPO bone-mimicking composition with double-network dynamic structure via the combined strategies of photo-crosslinking and dynamic self-assembly. The resulting engineered bionic matrix hydrogels with good hydrophilicity, mechanical and viscoelastic properties demonstrated excellent

recruitment, proliferation, osteogenic and angiogenic differentiation abilities *in vitro* and proper degradation rate with up to 28 days *in vivo*, which addresses the limitations of Matrigel, such as its rapid degradation and poor osteoinductivity, in the construction of bone organoids. Subsequently, BMSCs-loaded bionic matrix hydrogels with its long-term cell culture and self-mineralization were used to construct mineralized bone organoids via *in vitro* dynamic culture system. Remarkably, upon subcutaneous implantation in nude mice, the BMSCs-loaded bionic matrix hydrogels were evolved to vascularized bone organoids via *in vivo* heterotopic ossification for 4 weeks. Finally, this kind of engineered bionic matrix successfully facilitated efficient bone repair at the cranial defect sites in mice. These findings provide new insights for developing innovative matrix materials for bone organoid construction and offer promising strategies for both bone organoid development and the treatment of clinical bone defects.

2. Materials and methods

2.1. Synthesis and characterization

2.1.1. Synthesis of methacrylated dECM (mECM) hydrogel

Firstly, 1 g of dECM (Zhenghai, China) was dissolved in 75 % acetic acid (Aladdin, China) containing 10 mg of pepsin (Sigma, USA) at 50 °C to prepare the dECM solution. Subsequently, 287.5 mg (1.5 mmol) of EDC (Aladdin, China) and 172.5 mg (1.5 mmol) of NHS (Aladdin, China) were added to the dECM solution and mixed thoroughly using a magnetic stirrer. In a dark environment, methacrylic anhydride (MA) was introduced into the dECM solution, with the ratio of dECM (g) to MA (mL) kept at 1:3, and the reaction was left to continue for 24 h. Subsequently, the mixture underwent dialysis for one week in pure water at 37 °C, utilizing a dialysis membrane with a molecular weight cutoff (MWCO) of 500 Da. Finally, the dialyzed solution was lyophilized using a freeze dryer to obtain the mECM hydrogel. To confirm the composition of dECM, histological examination was conducted on tissue sections stained with H&E, Masson's trichrome, and Sirius red to verify the components of the dECM.

2.1.2. The preparation of DNA hydrogel

A 0.5 wt% salmon DNA solution (Sigma, USA) was prepared in TE buffer and incubated at 37 °C for 15 min to facilitate DNA hydrogel formation. The resulting hydrogel was then stained with GelRed dye (Life iLab, China), and its fluorescence was observed under ultraviolet (UV) excitation.

2.1.3. The preparation of CPO

The preparation method of CPO was adopted from previously reported studies [42]. First, 1.12 g of $CaCl_2{\cdot}2H_2O$ (Aladdin, China) was dissolved in 160 mL of ethanol. Under magnetic stirring, 22.2 mL of triethylamine (Aladdin, China) was added to the solution. Next, 0.4 mL of phosphoric acid (Aladdin, China) was mixed into 8 mL of ethanol and the resulting solution was stirred at normal temperature. The two solutions were subsequently combined and stirred magnetically for 12 h to allow the reaction to occur. The resulting product was centrifuged at 6000 rpm and lyophilized to obtain CPO. The morphology of CPO was analyzed using TEM and XRD was employed to examine the comparison.

2.1.4. Synthesis of mECM-DNA-CPO hydrogels

mECM (10 wt%), salmon DNA (0.5 wt%), and CPO (1 wt%) were dissolved in a PBS solution containing 0.25 wt% photoinitiator Lithium Phenyl-2,4,6-trimethylbenzoylphosphinate (LAP) at 60 °C. After complete dissolution, the solution was exposed to 405 nm UV light for 5–10 s to form the mECM-DNA-CPO. To confirm MA grafting, non-grafted dECM and mECM hydrogel powders were dissolved in heavy water and analyzed by nuclear magnetic resonance (NMR). The distribution of DNA in the mECM-DNA-CPO hydrogel was observed by staining the hydrogel in SYBR Green I. The interaction between CPO and mECM was characterized using Fourier transform infrared (FTIR) spectroscopy.

2.1.5. Characterization of mECM-DNA-CPO hydrogels

SEM was used to examine the hydrogel morphology. Samples were prepared and freeze-dried according to the methods described in the previous section. To enhance the conductivity of the material, the sample surfaces were coated with Au. The images were captured using a scanning electron microscope (JSM-7500F, Japan) at 5 kV magnification, and elemental analysis was performed using the integrated energy dispersive spectroscopy (EDS) system (AztecLive Ultim-Max 100, China). The hydrogel was evenly dropped onto a glass slide, followed by UV irradiation to induce gelation and obtain a stable hydrogel. Subsequently, the sample was placed on a contact angle goniometer, and 3 μL of distilled water was applied to the surface of the hydrogel. The contact angle between the water droplet and the hydrogel surface was immediately captured using a camera after the droplet made contact with the surface using a contact angle meter. After the hydrogel was completely swollen in PBS, its hardness was analyzed using a nano indentation instrument (unht3-bio step300 anton paar). After gelation of the hydrogel, small amplitude frequency sweep tests were performed at 37 °C to evaluate the storage modulus (G′), loss modulus (G″), and viscoelasticity within the frequency range of 0.01–100 rad/s. The swelling ratio of the hydrogel was measured by weight. The initial dry weight of the hydrogel (M_0) and its weight after swelling in PBS at room temperature (M_1) were recorded, ensuring excess surface water was removed with absorbent paper prior to weighing. The swelling ratio was determined using the following equation: Swelling ratio = $(M_1/M_0) \times 100$ %. To evaluate the degradation of the hydrogel, the initial mass of hydrogel degradation is M_0, then the hydrogel was submerged in PBS at 37 °C on a shaker. At different time intervals, the remaining hydrogel was freeze-dried and weighed (M_1). The residual mass of the hydrogel was calculated using the following equation: Residual mass = $[(M_0\text{-}M_1)/M_0] \times 100$ %. In the Ca^{2+} release experiment, mECM-DNA-CPO hydrogel was first prepared and placed in a centrifuge tube. An appropriate amount of PBS was added to completely immerse the sample, which was then incubated at 37 °C on a shaker at 100 rpm. At specified time intervals, 500 μL of the solution was sampled, and an equal volume of fresh PBS was added to replace it. The calcium ion concentration was measured using a Ca^{2+} detection kit (Beyotime, China).

2.2. In vitro cell analysis

2.2.1. Cell culture

Mouse BMSCs and HUVECs used in this study are derived from the same batch of commercial cell lines and obtained from OriCell (Shanghai, China), and all cell experiments were conducted using cells from passages 3 to 6. BMSCs and HUVECs were cultured in complete medium (MEM, Corning, USA) supplemented with 10 % fetal bovine serum (FBS, Sigma, USA) and 1 % penicillin-streptomycin (Gibco, USA), and in endothelial cell medium (ECM, Sciencell, USA), respectively. The cells were maintained at 37 °C in a 5 % CO_2 incubator, with the culture medium being replaced every two days, and the cells were cultured to the 3rd–6th passage for *in vitro* experiments.

2.2.2. Cell seeding in the hydrogels

In the subsequent cell experiments, BMSCs were seeded into the hydrogel at a concentration of 5×10^6 cells/mL. The BMSCs were resuspended in the hydrogel precursor solution, and the cell density was adjusted to the desired concentration. The cell-laden hydrogel precursor solution was poured into cylindrical molds and exposed to 405 nm ultraviolet light for 5–10 s to form the gel. The hydrogel was divided into three groups: (1) mECM, (2) mECM-DNA, and (3) mECM-DNA-CPO, for further studies. We first prepared the hydrogel extract. Specifically, the UV-cured hydrogel was repeatedly rinsed with PBS to remove unreacted residues. The hydrogel was then immersed in DMEM medium at a ratio of 1:10 (g/mL) and incubated at 37 °C for one week to ensure that all

soluble components of the hydrogel were fully dissolved. The resulting solution was subsequently filtered using a 0.22 μm membrane to obtain the hydrogel extract.

2.2.3. Cytotoxicity and proliferation assay

In all *in vitro* cell experiments, including those unrelated to osteogenic induction, such as CCK-8 assays and angiogenesis experiments, the CON group was cultured in basic medium without the addition of hydrogel extract. The distribution and viability of cells within the bionic matrix hydrogel were evaluated using live/dead cell staining. After seeding BMSCs in the hydrogels, cells were cultured for 1, 3, and 7 days. The cells were then treated with a Calcein AM/PI kit and incubated for 30 min, and cell viability was analyzed using a laser confocal scanning microscope (Olympus FV3000, Japan). Additionally, cell proliferation was evaluated using the CCK-8. After culturing cells in 96-well plates for 1, 3, and 7 days, the medium was then replaced with fresh medium containing 10 % CCK-8 reagent. The cells were incubated in a cell incubator, after which the absorbance of the supernatant at 450 nm was measured using a multifunctional microplate reader to assess cell proliferation. The MEM medium without BMSCs was used as the negative control, and the corresponding values were subtracted during data analysis.

2.2.4. Cytoskeleton and migration assay

To examine the scaffold morphology of BMSCs within the hydrogel, cells were stained with rhodamine-labeled phalloidin and DAPI on day 14 after seeding. Three-dimensional images were captured using a laser confocal scanning microscope to visualize cell morphology within the hydrogel. Additionally, a 24-well transwell co-culture system was used to assess the migration capability of BMSCs. BMSCs (2×10^4 cells) were seeded into the upper chamber, while 200 μL of hydrogel was placed in the lower chamber containing serum-free medium. After 12 h of incubation, the transwell chambers were stained with crystal violet. Migrated cells in the lower chamber were observed using an inverted microscope (Olympus, Japan) to evaluate BMSCs migration.

2.2.5. Alkaline phosphatase and alizarin red staining

In the *in vitro* osteogenic induction cell experiment, the CON group refers to cells cultured in osteogenic induction medium. BMSCs were plated in 24-well plates at a density of 2×10^4 cells per well. When the cells reached approximately 60 % confluence, the culture medium was substituted with osteogenic induction medium prepared using hydrogel extract, containing 10 mM β-glycerophosphate (β-GP, Sigma, USA), 50 μg/mL ascorbate-2-phosphate (Sigma, USA), and 10 nM dexamethasone (Sigma, USA). After staining, the wells were washed with PBS to remove excess dye, and images were captured using a microplate reader.

2.2.6. Angiogenesis assay

The hydrogel extract was prepared using the above method, and DMEM medium prepared with the extract was used to culture HUVECs for 24 h. Subsequently, tube formation and scratch assays were performed. Matrigel (50 μL, Corning, USA) was coated onto the bottom of a 96-well plate and incubated at 37 °C for 30 min to allow gelation. HUVECs were plated at a concentration of 2×10^4 cells per well onto the matrigel layer and incubated at 37 °C. At 4 h and 8 h after incubation, the cells were stained with Calcein AM, and images were captured using a fluorescence microscope. Tube formation was quantified using ImageJ software. The migration ability of HUVECs was detected by scratch test. HUVECs were seeded at a concentration of 1×10^5 cells per well. Once the cells reached 90 % confluence, the medium was replaced with serum-free medium, and the cells were starved for 12 h. Linear scratches were introduced into the monolayer using a sterile pipette tip. After 12 and 24 h of incubation with serum-free extracts from different hydrogels, the cells were stained with Calcein AM and then examined under a fluorescence microscope.

2.2.7. Quantitative real time polymerase chain reaction analysis

BMSCs and HUVECs were separately seeded into plates at a density of 2×10^5 cells and cultured for 7 days in osteogenic induction medium and ECM medium supplemented with hydrogel extract, respectively. Total RNA was extracted using the RNAiso Plus kit and then reverse-transcribed into cDNA using the reverse transcription kit (Takara, Japan). The expression levels of genes associated with osteogenesis and angiogenesis were quantified using qRT-PCR. The sequences of the primers used are listed in Tables S1 and S2. At the time of data processing, the CON group was normalized.

2.2.8. Western blot analysis

After 7 days of osteogenic induction of BMSCs within the hydrogel, proteins were extracted using RIPA lysis buffer. RIPA lysis buffer was supplemented with PMSF, protease inhibitors, and phosphatase inhibitors to prevent protein degradation. To prevent nonspecific protein binding, the samples were initially incubated with bovine serum albumin to block the surfaces. The samples were then incubated overnight at 4 °C with rabbit anti-COL I, anti-RUNX2, and anti-OCN antibodies (1:1000 dilution, Proteintech). Following this, the samples were incubated at room temperature for 2 h with goat anti-rabbit IgG H&L secondary antibody (1:10000, Servicebio). The samples were then detected using an enhanced chemiluminescence system. Finally, the expression levels of the target proteins were quantitatively analyzed using ImageJ software.

2.2.9. Transcriptomic analysis (mRNA-seq)

After 14 days of BMSC induction within the hydrogel, the hydrogel was cryo-fractured in liquid nitrogen, and total RNA was isolated from the cells using Trizol. The corresponding RNA library was prepared and subjected to high-throughput sequencing (GENE DENOVO, China). In this study, genes with a q-value below 0.05 and a fold change greater than 2 or less than 0.5 were regarded as exhibiting significant differential expression. Moreover, gene and pathway enrichment analysis were carried out using multiple analytical methods.

2.3. In vitro construction of bone organoids

BMSCs were embedded in mECM-DNA-CPO hydrogels and cultured under two different conditions: a static culture group in a 24-well plate and a dynamic culture group in an organ-on-a-chip system. These groups were designated as Static and Dynamic, respectively. In the two channels connected to the dynamic culture system, mECM-DNA-CPO hydrogel loaded with cultured BMSCs and osteogenic medium were placed, respectively. Gas was supplied at a flow rate of 12 BPM to provide sufficient force for the medium to circulate within the culture system, simulating the natural bone microenvironment. After culturing for 1, 2, 3, and 4 weeks, the samples were collected and scanned using a Micro-CT (Skyscan 1176, Bruker) to assess the mineralization ability of the organoids *in vitro*. Three-dimensional images were obtained using the micro-CT system at 65 kV and 80 μA. The three-dimensional images were reconstructed using NRecon software. Using CTAn software, a circular region with a diameter of 500 pixels was selected, and a section range of 100 ± 10 layers was chosen for mineralization parameter analysis. Additionally, tissue section staining was performed to verify the new bone formation capability.

2.4. In vivo construction of bone organoids

BMSCs were incorporated into different groups of hydrogels and subcutaneously injected into 4-6-week-old female BALB/C nude mice. After culturing for 2 and 4 weeks, the samples were collected and scanned using a micro-CT system to assess the *in vivo* mineralization capability of the bone organoids. Additionally, tissue section staining was conducted to assess new bone formation. To further assess the *in vivo* degradation ability of the hydrogels, we first soaked the hydrogels in a

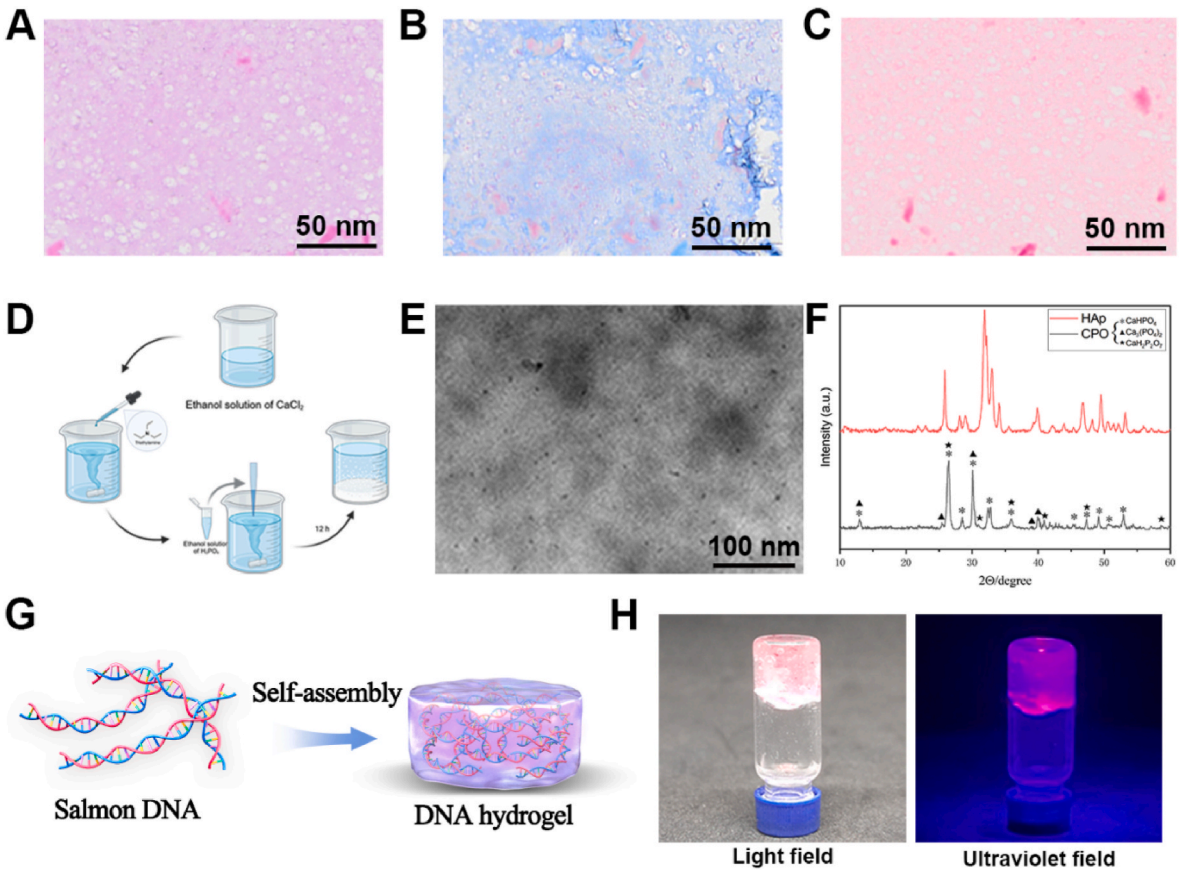

Fig. 1. Component analysis of bionic matrix hydrogel. (A–C) H&E, Masson, and Sirius Red Staining of dECM. (D) Schematic diagram of CPO preparation. (E) TEM images of CPO. (F) XRD analysis of CPO. (G) Schematic diagram of DNA self-assembly into hydrogel. (H) Gelred-stained DNA hydrogel.

Cy5.5 NHS solution (DuoFluor, China) for 1 h to label the hydrogels, followed by rinsing with PBS to remove excess dye. The labeled hydrogels were then implanted into the dorsal region of C57BL/6 mice. The *in vivo* retention of the hydrogels was monitored using an *in vivo* imaging system (AniView100, China), with excitation and emission wavelengths set to 675 nm and 740 nm, respectively.

2.5. In vivo osteogenesis evaluation

2.5.1. Mice cranial defect model and Micro-CT analysis

Animal experiments were conducted in accordance with the guidelines approved by the ethics committee of Shanghai University. Critical-sized bone defects were created in 6–8-week-old male C57BL/6 mice for in *vivo* osteogenesis studies. Under general anesthesia with pentobarbital sodium, a 3 mm diameter cranial defect was created on the right side of the mouse cranial using a circular saw. The hydrogel containing BMSCs was then implanted into the defect site, and the wound was sutured. The experiment was categorized into four groups: (1) CON group; (2) mECM hydrogel group; (3) mECM-DNA hydrogel group and (4) mECM-DNA-CPO hydrogel group. In animal experiments, the CON group, only the cranial defect procedure was performed, without any additional interventions. Mice were euthanized at six- and twelve-weeks post-surgery, and their cranials were collected and fixed in 4 % paraformaldehyde. Subsequently, three-dimensional images were obtained using a micro-computed tomography system at 50 kV and 60 μA. The images were reconstructed using NRecon software, and parameters related to new bone formation were analyzed using CTAn software.

2.5.2. Histological and immunohistochemical staining

The mice cranials samples were decalcified in a 10 % EDTA solution (Servicebio, China) for 4 weeks. Subsequently, the underwent dehydration through a stepwise ethanol series, followed by paraffin embedding before sectioning. H&E staining and Masson's trichrome staining were performed to analyze the cells and tissue's structure. Immunohistochemistry was used to detect the expression of COL I, while immunofluorescence was employed to assess the expression of OCN and CD31, assessing new bone formation and angiogenesis. After 12 weeks post-surgery, the heart, liver, kidney, spleen, and lungs of the mice were collected and subjected to pathological staining to evaluate the biocompatibility of the bone organ constructs.

2.6. Statistical analysis

Experimental data were analyzed using GraphPad Prism software. All experimental results were obtained from a minimum of three independent experiments and are expressed as the mean ± standard deviation (SD). Comparisons between multiple groups were conducted using one-way analysis of variance (ANOVA). Statistical significance was considered for p values ≤ 0.05.

3. Results and discussion

3.1. Preparation and characterization of bionic matrix hydrogel components

First, the individual components of the bionic matrix hydrogel were prepared and characterized. dECM consists of a variety of proteins that confer tissue-specific physiological functions. Numerous studies have elucidated the intricate protein composition of bone-derived dECM. In this study, dECM was obtained from the femur of pigs. We employed histological staining to validate the components of dECM. H&E staining confirmed the successful removal of cells, cell debris, and nuclei from

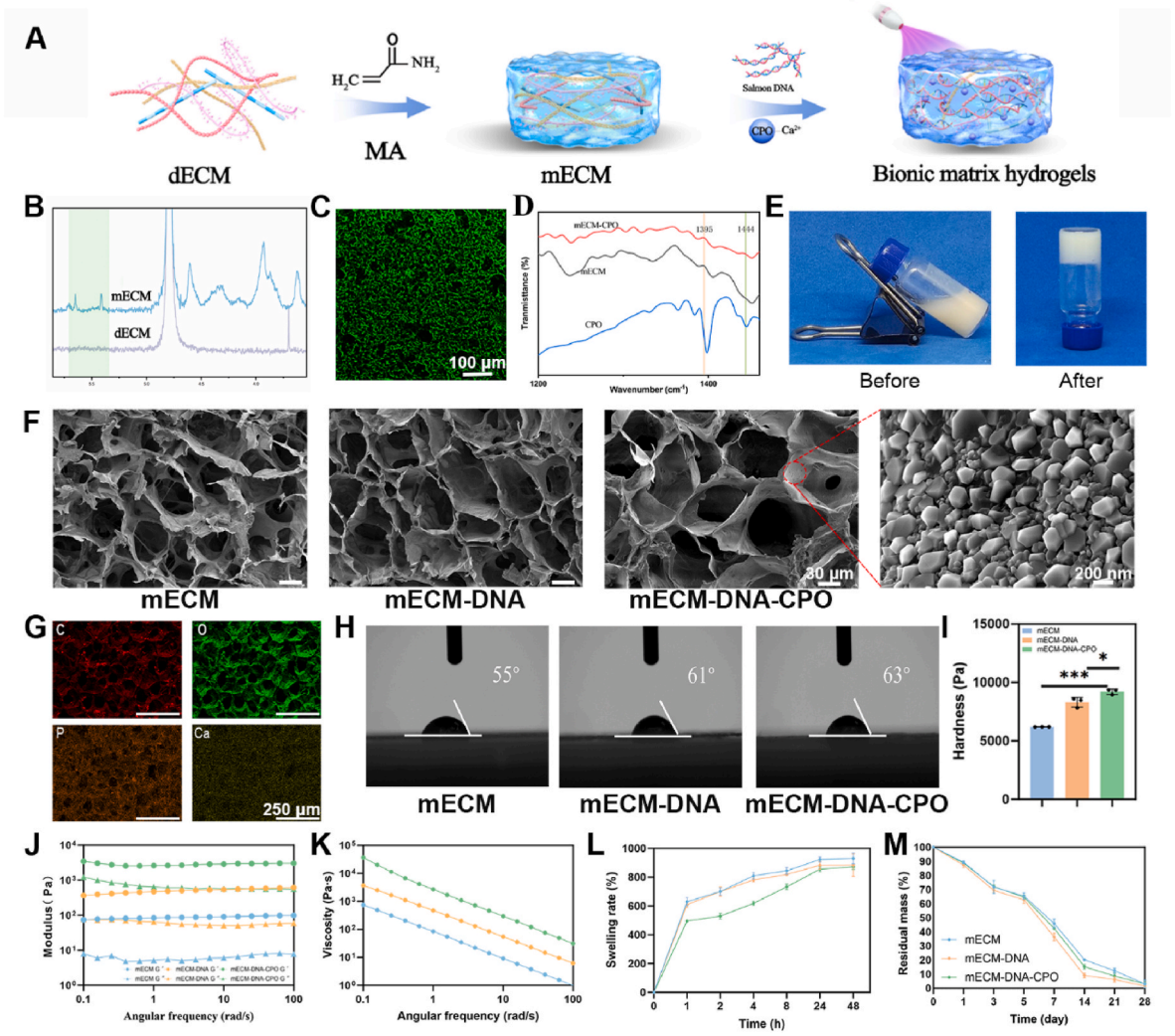

Fig. 2. Preparation process and performance characterization of bionic matrix hydrogel. (A) Schematic diagram of mECM-DNA-CPO preparation. (B) ^{1}H NMR spectrogram of mECM and dECM. (C) Staining of DNA network with SYBR Green I. (D) FTIR spectra of bionic matrix hydrogel. (E) The image before and after gelation. (F) SEM images of bionic matrix hydrogel. (G) EDS images of bionic matrix hydrogel. (H) Hydrophilic contact angle of bionic matrix hydrogel. (I) Hardness of bionic matrix hydrogel. (J–K) Rheological analysis and viscoelastic properties of bionic matrix hydrogel. (L) The swelling ratio of bionic matrix hydrogel in PBS. (M) Residual mass of the biomimetic matrix hydrogel in PBS at 37 °C *in vitro*. All data were obtained from a minimum of n = 3 independent experiments and are expressed as mean ± SD. **P < 0.01, ***P < 0.001 compared to Blank group.

dECM (Fig. 1A). Additionally, Masson's trichrome staining and sirius red staining demonstrated the presence of abundant collagen in the dECM (Fig. 1B–C). Collagen, particularly type I collagen (COL I), is a key component of the skeleton [46]. Its regular triple-helix structure provides nucleation sites for the deposition and growth of inorganic minerals. In the previous study, we established the preparation method for CPO (Fig. 1D). Transmission electron microscopy (TEM) imaging showed that CPO was a nanoparticle with uniform size (Fig. 1E). X-ray diffraction (XRD) analysis indicates that CPO was the mixture of $CaHPO_4$, $Ca_3(PO_4)_2$ and $CaH_2P_2O_7$ phases, providing a foundation for *in-situ* biomimetic mineralization of hydroxyapatite (HAp) resembling bone in mineralized bone construction (Fig. 1F). Furthermore, the Ca^{2+} not only provide nucleation sites for the biomineralization of bone organoids but also promote angiogenesis. The maximum cell viability was observed when the CPO content was 1 wt %. Therefore, a CPO concentration of 1 wt % was selected for the construction of the hydrogel (Fig. S1). Salmon DNA, as a natural long-chain DNA, can self-assemble into DNA hydrogels through base complementary pairing (Fig. 1G). The DNA hydrogel was stained with GelRed, and red fluorescence emitted by the DNA within the hydrogel was observed (Fig. 1H). The negative charges, particularly the phosphate groups, in the DNA hydrogel, can form coordination complexes with CPO, thereby promoting mineral nucleation. These results indicate that the preparation of all components has been successfully completed, laying the foundation for the fabrication of the bionic matrix hydrogel.

3.2. Fabrication and characterization of bionic matrix hydrogel

The construction of bone organoids requires a culture matrix that provides a biomimetic microenvironment. Through the modification and interaction of its components, a mECM-DNA-CPO hydrogel was developed to replicate the bone microenvironment (Fig. 2A). First, dECM was modified by adding MA, resulting in the formation of mECM hydrogel. Under the irradiation of 405 nm ultraviolet light, the mECM hydrogel precursor solution reacted with the photoinitiator LAP to achieve the transition from liquid to gel state. As shown in Fig. 2B, ^{1}H NMR analysis revealed that new characteristic peaks between about 5.3 and 6.2 ppm appeared in mECM group, which refers to the protons of methacrylate vinyl group of MA (Fig. 2B). Next, we added salmon DNA to the ungelled mECM precursor solution to form the mECM-DNA hydrogel. To verify the distribution of DNA within the hydrogel, we stained the DNA using SYBR Green I. The results showed that the DNA

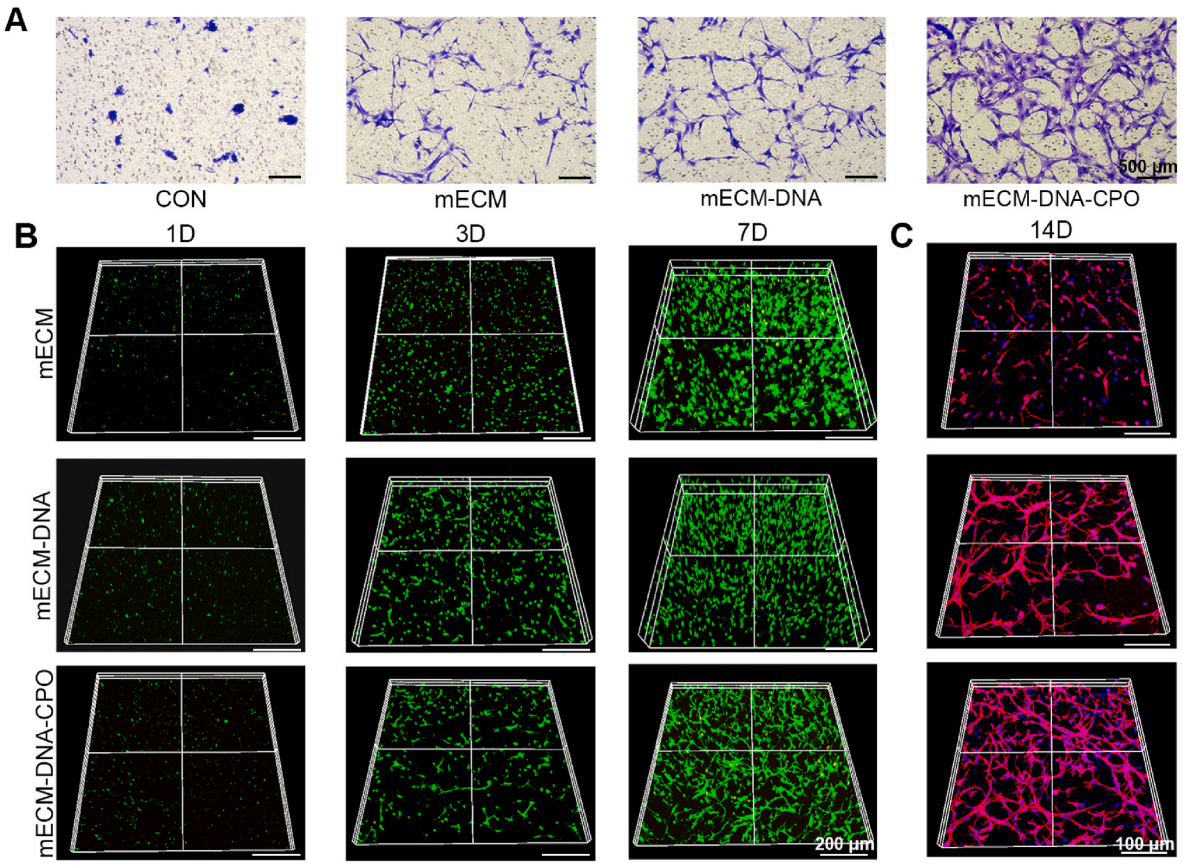

Fig. 3. Cellular behavior of bionic matrix hydrogel. (A) Recruitment of BMSCs by bionic matrix hydrogel. (B) Distribution and live/dead analysis of BMSCs in bionic matrix hydrogel. (C) Cytoskeletal network of BMSCs in bionic matrix hydrogel. All data were obtained from a minimum of n = 3 independent experiments and are expressed as mean ± SD. **P < 0.01, ***P < 0.001 compared to Blank group.

was evenly distributed throughout the mECM-DNA hydrogel, confirming that the dECM and DNA form a uniform and interwoven dual network within the mECM-DNA hydrogel (Fig. 2C). Next, we added CPO to the mECM-DNA, where the Ca^{2+} in CPO interact strongly with the carboxyl groups in mECM, facilitating their connection. To verify the successful incorporation of CPO, FTIR analysis was conducted. Both the mECM and mECM-CPO groups exhibited a typical peak at around 1395 cm^{-1}, corresponding to the C-O stretching vibration of the carboxyl group. Notably, mECM-CPO group also displayed a peak at 1444 cm^{-1}, which is attributed to the interaction between Ca^{2+} and the carboxyl groups in mECM (Fig. 2D). To verify the formation of the mECM-DNA-CPO hydrogel, an inversion test was performed. After exposure to 405 nm UV light for 5–10 s, the mECM-DNA-CPO successfully transitioned from a liquid to a gel state. (Fig. 2E).

After the successful preparation of the mECM-DNA-CPO hydrogel, its characteristics were analyzed using various methods. The SEM images show that the freeze-dried mECM, mECM-DNA, and mECM-DNA-CPO hydrogels all exhibit a uniform porous structure with similar pore sizes (Fig. 2F). This porous structure facilitates cell migration and adhesion. Additionally, cross-linked CPO was observed within the mECM-DNA-CPO hydrogel. Compared to CPO alone, the morphology of CPO in mECM-DNA-CPO appeared altered, with a more heterogeneous size distribution, likely due to the aggregation of CPO during its interaction with mECM. Through porosity analysis, it was found that the addition of salmon DNA increased the porosity of the hydrogel. This may be attributed to the double network formed by the self-assembly of salmon DNA, which enlarged the pore size of the hydrogel (Fig. S2). EDS analysis revealed a uniform distribution of elements throughout the hydrogel. Moreover, compared to the mECM group, the mECM-DNA-CPO group exhibited an increased and evenly distributed presence of Ca elements, confirming the uniform crosslinking of CPO within the hydrogel (Fig. 2G and S3). The hydrophilicity of the hydrogel was verified through contact angle measurements (Fig. 2H). Following the addition of DNA and CPO, the hydrophilicity of the hydrogel slightly decreased, although the difference was not statistically meaningful. This is likely attributed to the lower hydrophilicity of DNA hydrogels and CPO compared to mECM. Additionally, the incorporation of DNA and CPO resulted in a gradual increase in the stiffness of the hydrogel (Fig. 2I). Since bone organoids require mechanical support, the enhanced stiffness of mECM-DNA-CPO provides a significant advantage for their formation. Rheological analysis revealed that, across a frequency range of 0.01–100 rad/s, the elastic shear storage modulus (G') consistently exceeded the viscous shear loss modulus (G''), indicating that the hydrogel preserved a relatively stable structure. Moreover, the addition of DNA and CPO resulted in an increase in G', which enhanced the elasticity of both mECM-DNA and mECM-DNA-CPO hydrogels (Fig. 2J). This observation was further validated by analyzing the viscoelastic profiles obtained from the rheological experiments (Fig. 2K). The high viscoelasticity of the hydrogel more closely mimics the mechanical microenvironment of the ECM, facilitating the rearrangement and self-healing of hydrogel molecules. The swelling ratio and degradation rate of the samples were evaluated by weighing. In the swelling experiment, all samples displayed similar behavior, reaching swelling equilibrium at approximately 24 h with a swelling ratio of around 900 %. However, the mECM-DNA-CPO group showed slower swelling during the first 8 h compared to the other hydrogels, which is likely attributed to the presence of CPO in the mECM-DNA-CPO (Fig. 2L). In addition, degradation performance is a crucial role in the practical application of biomaterials for organoid construction. All samples exhibited similar degradation behaviors, with no statistically

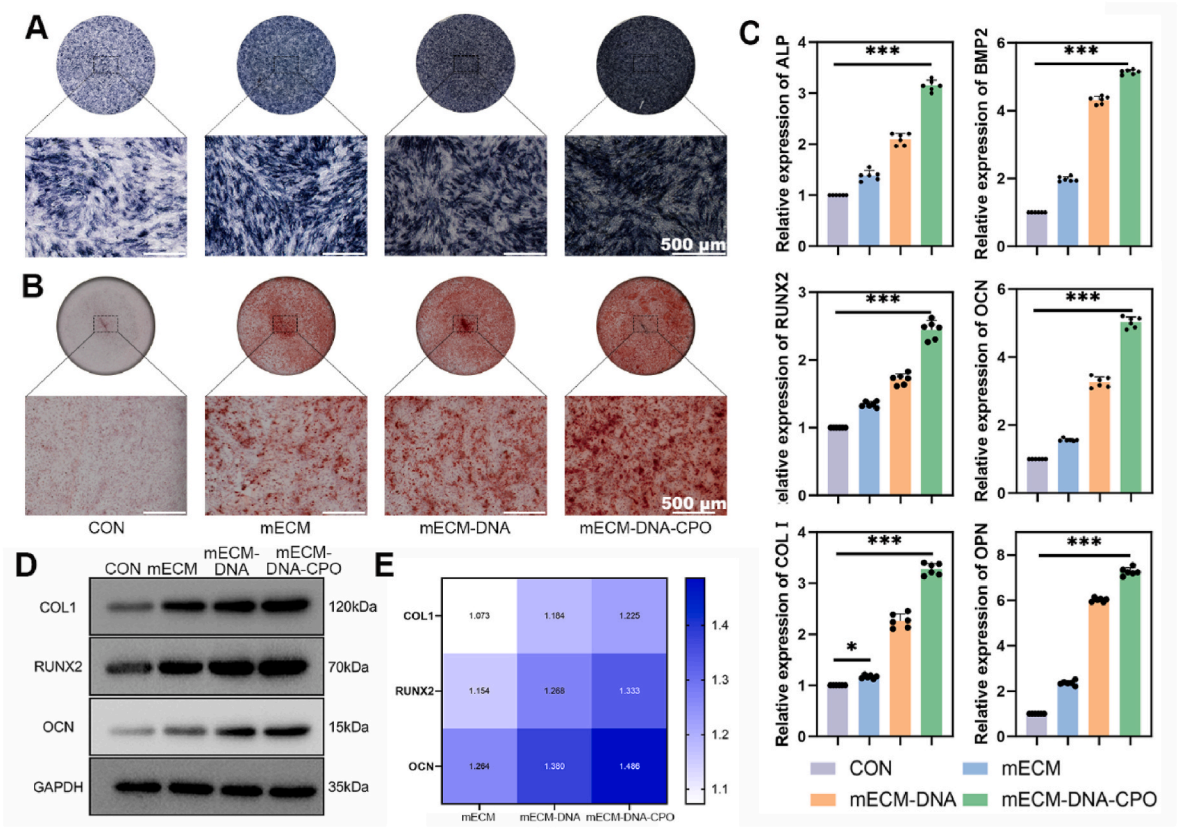

Fig. 4. Verification of osteogenic mineralization functionality of bionic matrix hydrogel *in vitro*. (A) ALP staining of BMSCs cultured in bionic matrix hydrogel for 7 days. (B) ARS staining of BMSCs cultured in bionic matrix hydrogel for 14 days. (C) Changes in ALP, BMP2, RUNX2, OCN, COL I, and OPN after co-culture of BMSCs with bionic matrix hydrogel. (D–E) Changes and quantitative analysis of COL I, RUNX2, and OCN proteins. All data were obtained from a minimum of n = 3 independent experiments and are expressed as mean ± SD. **P < 0.01, ***P < 0.001 compared to Blank group.

significant differences. However, the mECM-DNA group exhibited slightly more degradation, with approximately 7.83 % of the sample remaining after 28 days. In comparison to the mECM group, the DNA in the mECM-DNA group exhibited a greater tendency to degrade. However, the degradation rate of the mECM-DNA-CPO group was between that of the mECM and mECM-DNA groups, which may be attributed to the addition of CPO, which interacts with mECM and slows down the hydrogel's degradation (Fig. 2M). While *in vitro* degradation experiments provide insights into the hydrogel's degradation time, the degradation time observed *in vitro* does not directly correlate with *in vivo* degradation due to factors such as biomineralization and tissue growth. In addition, the results of the calcium ion release experiment show that the release of calcium ions in PBS remained uniform during the first 14 days. However, after 14 days, the release rate of calcium ions slightly slowed down, but it remained rapid (Fig. S4). The diverse properties of this biomimetic matrix hydrogel make it highly suitable for subsequent cell culture and differentiation, playing a pivotal role in facilitating cellular processes.

3.3. Cellular behavior of the bionic matrix hydrogel

Cell viability, adhesion, and proliferation within the hydrogel are crucial for organoids formation. First, the recruitment ability of the hydrogel for BMSCs was assessed using the transwell experiment (Fig. 3A and S5A). Compared to the CON group, the hydrogel significantly enhanced the migration ability of BMSCs, demonstrating its effectiveness in recruiting BMSCs. Notably, in the transwell experiment, since the BMSCs did not directly contact the hydrogel, cell recruitment was primarily attributed to ions released by the hydrogel. Subsequently, the proliferation capacity of BMSCs was assessed using the CCK-8 assay after 1, 3, and 7 days of exposure to the hydrogel extract (Fig. S5B). As the culture time increased, the OD values gradually rose, indicating that the number of BMSCs increased with proliferation. Moreover, no statistically significant differences were observed between the groups at any time point, indicating outstanding cell compatibility. Furthermore, live/dead staining of BMSCs cultured in the bionic matrix hydrogel in a three-dimensional environment revealed that the BMSCs were evenly distributed within the hydrogel with very few dead cells. An interesting phenomenon was also observed: initially, the cells were uniformly distributed within the hydrogel and exhibited an oval shape. However, over time, the pseudopodia of the BMSCs extended outward, eventually forming a complex three-dimensional network (Fig. 3B). After 14 days of culture, cytoskeleton staining of the BMSCs revealed the formation of this three-dimensional network. In the mECM hydrogel, the BMSCs cytoskeleton was not fully spread, while in the mECM-DNA and mECM-DNA-CPO groups, a well-defined three-dimensional network was observed (Fig. 3C). The formation of a cellular network facilitates the establishment of connections within the three-dimensional space, which not only supports cell aggregation but also promotes signal transmission between cells and between cells and the matrix. This is highly important for the development and functional implementation of bone organoids. These results demonstrate that this novel bionic matrix hydrogel can support the long-term culture of BMSCs, establishing a foundation for its role promoting BMSCs osteogenic differentiation and HUVEC angiogenesis, thereby facilitating the construction of bone organoids.

3.4. Effect of bionic matrix hydrogel on osteogenic differentiation of BMSCs

After characterizing the cell compatibility and scaffold morphology

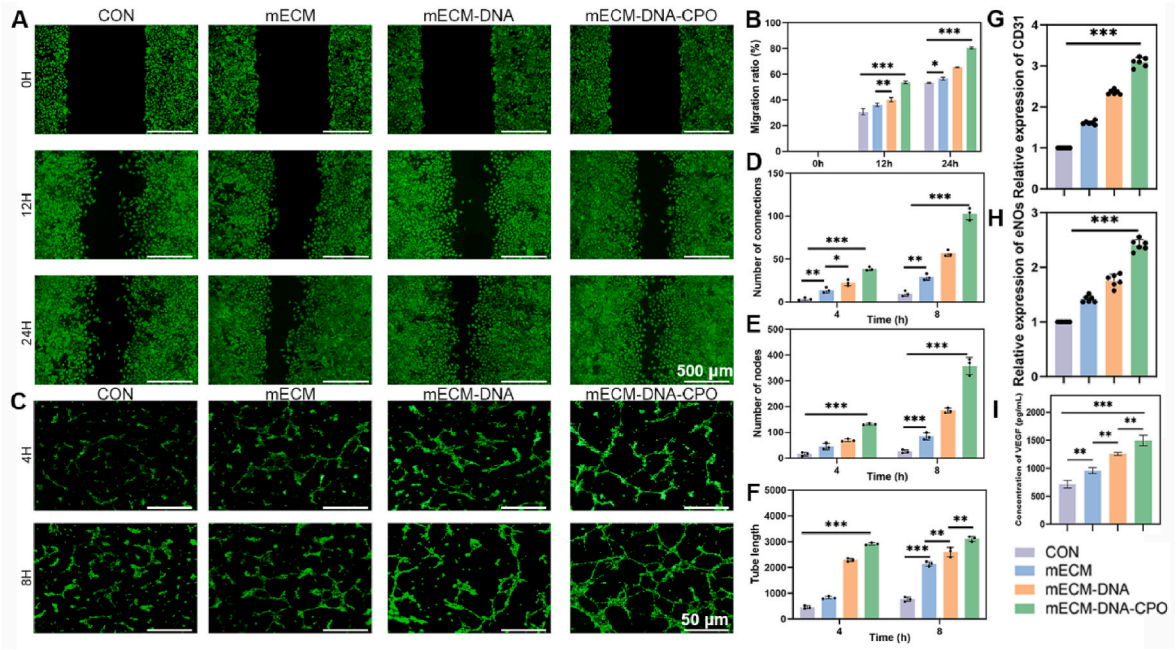

Fig. 5. Functional verification of angiogenesis promotion by bionic matrix hydrogel *in vitro*. (A–B) Migration assay and quantitative analysis of HUVECs. (C–F) Tube formation assay and quantitative analysis of HUVECs. (G–H) Changes in eNOS and CD31 after 7 days of co-culture of HUVECs with bionic matrix hydrogel. (I) Changes in VEGF levels in the supernatant after 7 days of co-culture of HUVECs with bionic matrix hydrogel. All data were obtained from a minimum of n = 3 independent experiments and are expressed as mean ± SD. **P < 0.01, ***P < 0.001 compared to Blank group.

of the bionic matrix hydrogel with BMSCs, we further examined its impact on enhancing osteogenic differentiation. The osteogenic differentiation is marked by the expression of alkaline phosphatase (ALP) in the early stage and alizarin red staining (ARS) in the late stage. After 7 days of BMSCs differentiation, ALP staining showed gradually increasing intensity in the mECM, mECM-DNA, and mECM-DNA-CPO groups (Fig. 4A and S6A). ARS binds to calcium deposits by chelating with Ca^{2+}, serving as an indicator of late-stage osteogenic mineralization. After 14 days of BMSCs differentiation, ARS staining showed a marked increase in mineral deposition in the mECM group compared to the CON group. Notably, the mECM-DNA-CPO group exhibited the highest level of calcium deposition, aligning with the ALP staining results. These findings confirm the osteogenic potential of the bionic matrix hydrogel (Fig. 4B and S6B). Furthermore, the expression levels of osteogenic markers, including ALP, BMP2, COL I, RUNX2, OCN, and OPN, were measured using qRT-PCR after 7 days of culture (Fig. 4C). The results demonstrated a significant increase in the expression of osteogenic differentiation-related genes on day 7, corresponding to changes in the culture matrix. This finding indicates that the novel matrix hydrogel effectively enhances osteogenic differentiation at the genetic level. To further confirm the expression of related proteins, Western blotting was performed. The results indicated that the expression levels of osteogenic proteins, including COL I, RUNX2, and OCN, were significantly elevated in the mECM-DNA-CPO group compared to the other groups (Fig. 4D–E). This further confirms that mECM-DNA-CPO not only promotes osteogenesis at the genetic level but also enhances the expression of osteogenic proteins at the protein level. In conclusion, we demonstrate that this bionic matrix hydrogel can construct a bone microenvironment similar to natural bone, accelerating the osteogenic mineralization process of BMSCs. This highlights its potential as an excellent substrate for bone organoid construction.

3.5. Effect of bionic matrix hydrogel on angiogenesis of HUVECs

Vascular regeneration is a crucial process in bone tissue regeneration, as an adequate blood supply ensures the delivery of essential nutrients and oxygen to support bone tissue repair and growth. Therefore, the development of vascularized bone organoids represents a promising and innovative approach for constructing functional bone organoids. Studies have shown that the natural proteins in mECM, as well as the Ca^{2+} released from CPO, can stimulate endothelial cells to secrete angiogenesis-related growth factors, thereby accelerating endothelial cell proliferation and angiogenesis [47]. To explore the effect of mECM-DNA-CPO on angiogenesis, we conducted relevant experiments using HUVECs. First, we evaluated the proliferation ability of HUVECs using the CCK-8 assay (Fig. S7). As the culture time increased, the OD values gradually increased, indicating that the hydrogel exhibited no toxicity toward HUVECs. The migration ability of HUVECs was further evaluated using a scratch assay (Fig. 5A–B). Both mECM, mECM-DNA, and mECM-DNA-CPO accelerated the migration of HUVECs toward the wound area. Notably, the mECM-DNA-CPO group exhibited a significantly faster wound healing rate compared to the other groups. The accelerated recruitment of endothelial cells facilitates the formation of new blood vessels in vascularized bone organoids and expedites the process of vascularized bone repair in bone tissue. Tube formation assays showed that both mECM-DNA and mECM-DNA-CPO groups formed distinct circular lumen structures within 4 h. By 8 h, a well-defined vascular network was observed in the mECM-DNA-CPO group (Fig. 5C). Quantitative analysis demonstrated a gradual increase in the number of branching points, tube formation, and tube length from the CON group to the mECM-DNA-CPO group (Fig. 5D–F). To evaluate the regulatory effect of the hydrogel on angiogenesis at the genetic level, the expression of angiogenesis-related genes was examined. Both eNOS and CD31 expressions were increased (Fig. 5G–H). ELISA measurements of VEGF concentration in the supernatant from different experimental groups exhibited a similar trend (Fig. 5I). The excellent pro-angiogenic ability of this bionic matrix hydrogel holds substantial significance for the construction of vascularized bone organoids.

3.6. Transcriptome analysis of BMSCs in bionic matrix hydrogels

To further investigate the effects of this novel bone-mimetic matrix hydrogel on BMSCs, mRNA sequencing (mRNA-seq) was performed to analyze gene expression. Principal component analysis (PCA) revealed

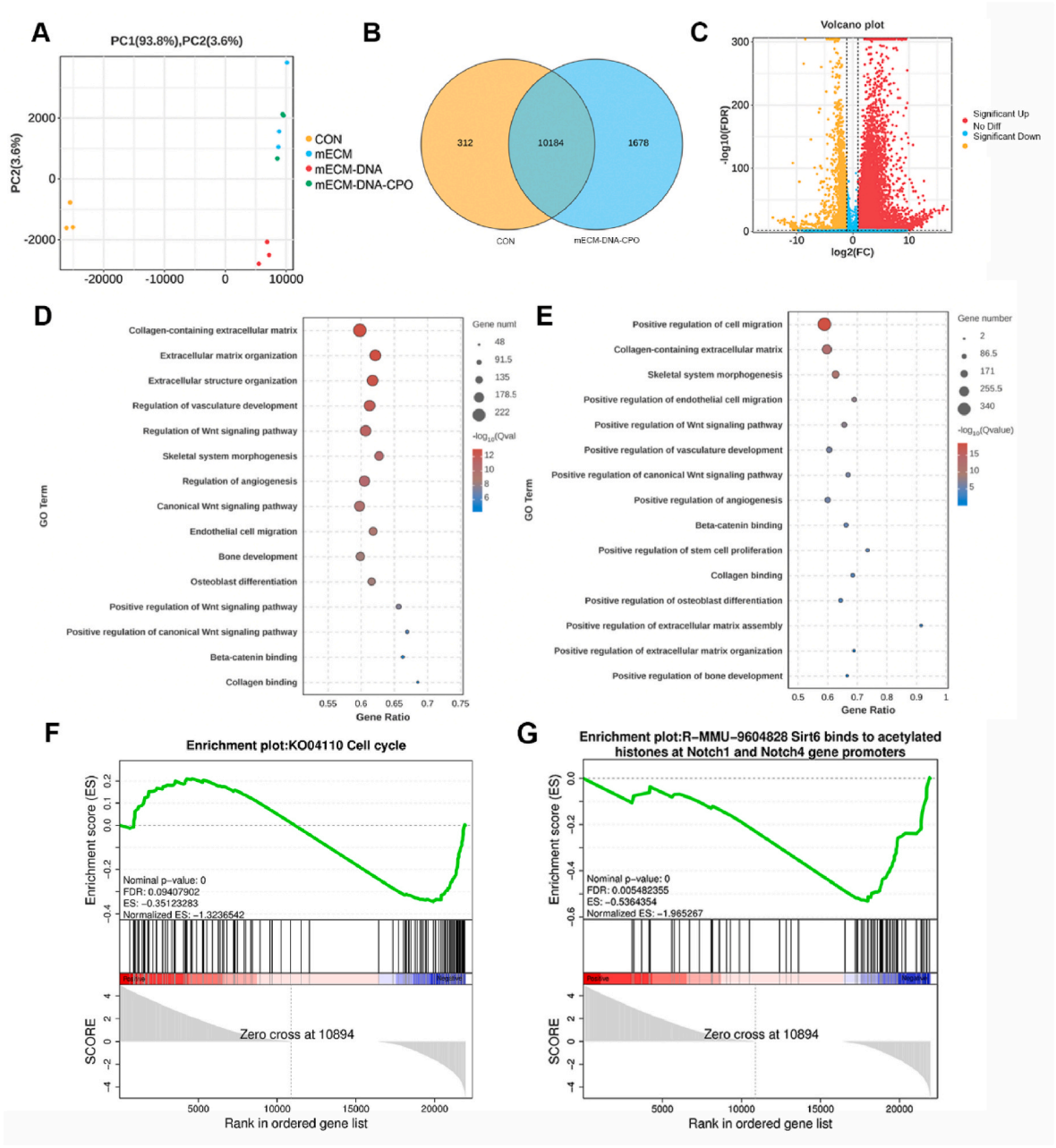

Fig. 6. Transcriptomic analysis. (A) PCA of DEGs between the CON and mECM-DNA-CPO groups. (B) Comparison of mRNA expression levels between the CON and mECM-DNA-CPO groups. (C) Volcano plot representation of genes exhibiting significant expression changes exceeding a 2-fold difference. (D) GO analysis of upregulated gene. (E) KEGG pathway analysis of upregulated gene. (F–G) GSEA analysis.

high reproducibility among the samples, with significant differences between the groups, indicating the reliability of the transcriptome data (Fig. 6A). Analysis revealed that the mECM-DNA-CPO group exhibited 1990 differentially expressed genes (DEGs) compared to the CON group, including 312 upregulated and 1678 downregulated genes (Fig. 6B). A volcano plot was used to display the distribution of significantly changed DEGs (Fig. 6C). Additionally, we performed gene ontology (GO) analysis on the upregulated genes, classifying DEGs into biological processes, cellular components, and molecular functions. Compared to the CON group, the mECM-DNA-CPO group exhibited significant upregulation of genes associated with biological processes such as ECM production, cell migration, cell proliferation, osteogenic differentiation, and angiogenesis. Similarly, genes related to molecular functions, including biomolecular activity and collagen binding, were also significantly upregulated (q-value <0.05 and $0.6 < |\log2FC| < 1$) (Fig. 6D). Next, Kyoto Encyclopedia of Genes and Genomes (KEGG) pathway enrichment analysis was performed revealing significant upregulation of osteogenesis-related signaling pathways, such as Wnt signaling, cell proliferation, and extracellular matrix development pathways (Fig. 6E). We further conducted GSEA analysis, which revealed that mECM-DNA-CPO significantly upregulated cell cycle progression while downregulating the acetylation of histones bound to the promoters of Sirt6, Notch1, and Notch4 genes [48] (Fig. 6F–G). Analysis of these two pathways revealed that moderate enhancement of the cell cycle promotes BMSCs proliferation and accelerates the mineralization of bone organoids [49]. Additionally, Sirt6, as an acetylated protein binding to the promoters of Notch1 and Notch4 genes [50,51], when downregulated, increases the expression of Notch1 and Notch4, thereby upregulating the Notch signaling pathway, which in turn accelerates osteogenic differentiation and angiogenesis [52]. In conclusion,

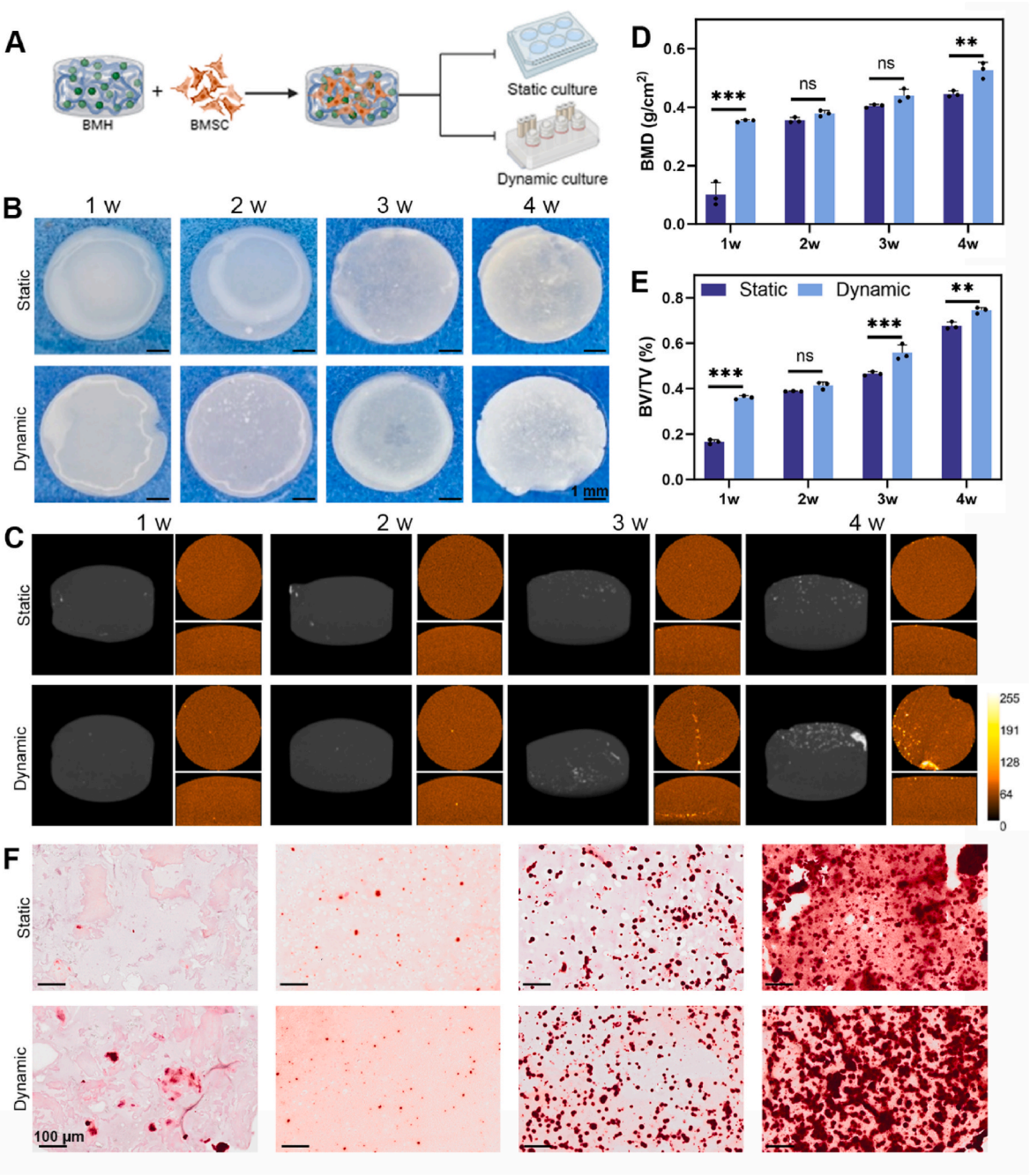

Fig. 7. Construction of mineralized bone organoids via *in vitro* dynamic culture. (A) Schematic diagram of dynamic *in vitro* construction of bone organoids. (B) Macroscopic images of bone organoids constructed via dynamic *in vitro* culture. (C–E) 3D reconstruction and quantitative analysis of bone organoids cultured dynamically *in vitro*. (F) ARS staining images of bone organoids constructed via dynamic *in vitro* culture. All data were obtained from a minimum of n = 3 independent experiments and are expressed as mean ± SD. **P < 0.01, ***P < 0.001 compared to Blank group.

mECM-DNA-CPO enhances osteogenic differentiation and angiogenesis of BMSCs by accelerating cell proliferation and migration, significantly increasing ECM synthesis, and improving cell adhesion to the ECM. These results indicate that mECM-DNA-CPO exhibits excellent osteogenic and pro-angiogenic capabilities, providing a favorable biomimetic matrix environment for the subsequent construction of bone organoids.

3.7. Bionic matrix hydrogels to construct bone organoids in vitro

To verify the ability of the bionic matrix hydrogel to construct self-mineralizing bone organoids *in vitro*, we cultured mECM-DNA-CPO hydrogel containing BMSCs under both static culture and dynamic organoid culture system conditions (Fig. 7A). The dynamic culture system consists of two connected culture wells and channels. One well is designated for the organoids, while the other contains the culture medium. Bone organoids were cultured using a set gas flow rate of 12 BPM (Fig. S8). In the organoid culture system, dynamic fluid flow provides a uniform distribution of nutrients and oxygen, while also eliminating metabolic waste. This creates a microenvironment that more closely mimics *in vivo* conditions, facilitating the construction of bone organoids. This system better simulates the interactions between cells, the extracellular matrix, and the surrounding environment, which enhances the mineralization rate of the bone organoids. With increasing culture time, the former bone organoids gradually became transparent, and

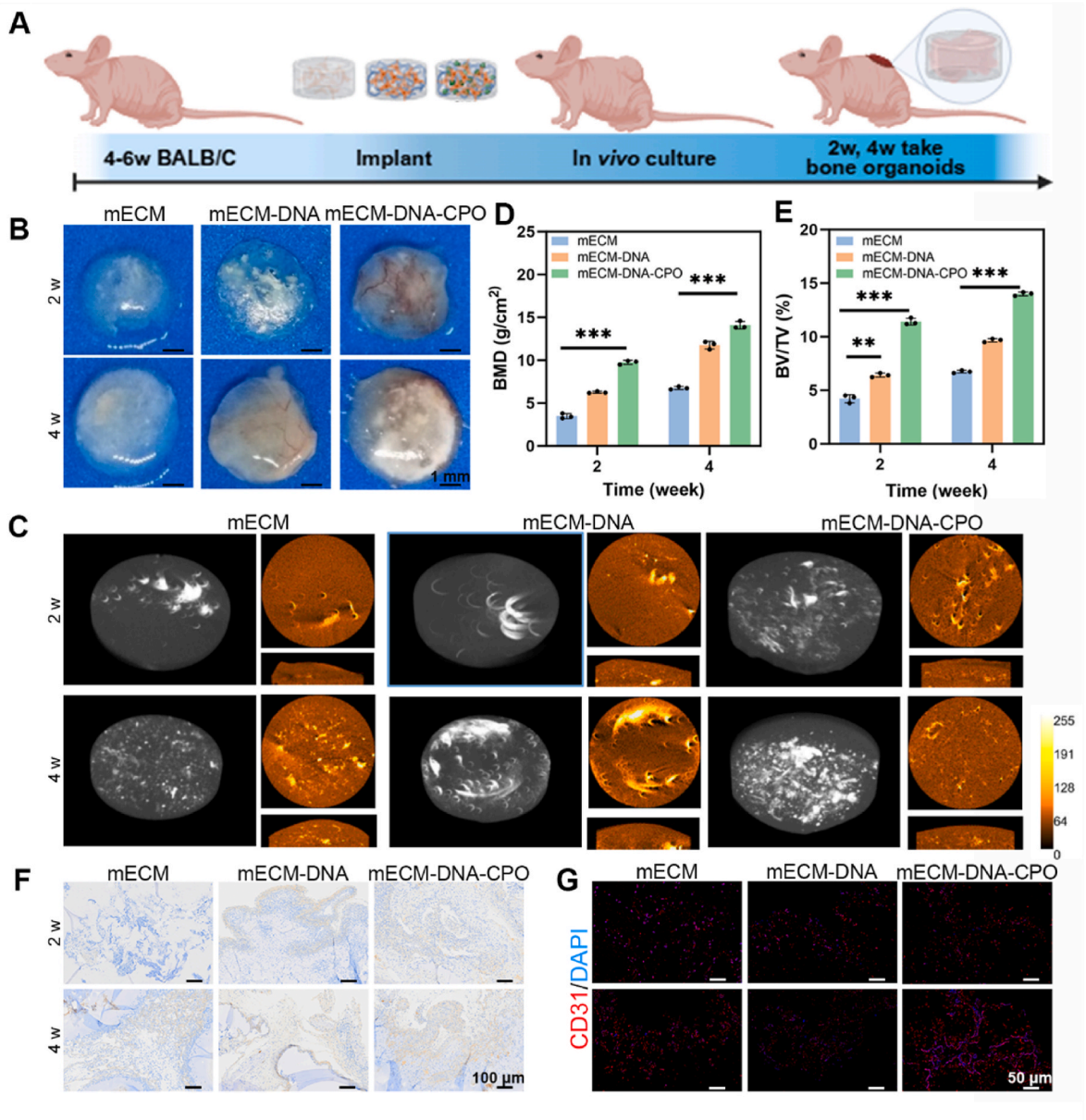

Fig. 8. Construction of vascularized bone organoids using bionic matrix hydrogel via *in vivo* heterotopic ossification. (A) Schematic diagram of *in vivo* ectopic mineralization and construction of vascularized bone organoids. (B) Macroscopic images of vascularized bone organoids constructed via *in vivo* ectopic mineralization. (C–E) 3D reconstruction and quantitative analysis of vascularized bone organoids constructed via *in vivo* ectopic mineralization. (F) COL I staining of vascularized bone organoids constructed via *in vivo* ectopic mineralization. (G) CD31 staining of vascularized bone organoids constructed via *in vivo* ectopic mineralization. All data were obtained from a minimum of n = 3 independent experiments and are expressed as mean ± SD. **P < 0.01, ***P < 0.001 compared to Blank group.

visible white calcium deposits were clearly observed by the naked eye (Fig. 7B). Micro-CT analysis revealed a significant increase in mineral deposition within the bone organoids as culture time progressed. Additionally, mineral deposition was slightly greater in the dynamic culture system compared to the static culture (Fig. 7C). Analysis of bone mineral density (BMD) and bone volume-to-tissue volume ratio (BV/TV) further confirmed that bone organoid formation was slightly enhanced under dynamic culture conditions compared to static culture, highlighting the suitability of dynamic culture for bone organoid construction (Fig. 7D–E). H&E staining of bone organoids cultured for four weeks revealed that BMSCs were uniformly distributed within the organoids (Fig. S9). With the increase in culture time, the calcification deposition within the organoids gradually increased. During the first 2 weeks of culture, no notable difference in calcification deposition was observed between the Dynamic and Static groups. Nevertheless, after 3 weeks of culture, the calcification deposition in the Dynamic group was slightly higher than in the Static group, with the difference becoming more pronounced at 4 weeks (Fig. 7F). We hypothesize that with extended culture time, the dynamic culture system exhibits a more pronounced effect in promoting bone organoid formation. These results highlight the pivotal role of mECM-DNA-CPO hydrogel in bone organoid construction and introduce a novel culture system for *in vitro* bone organoid formation. Improvements in the culture system offer new insights and strategies for advancing bone organoid construction.

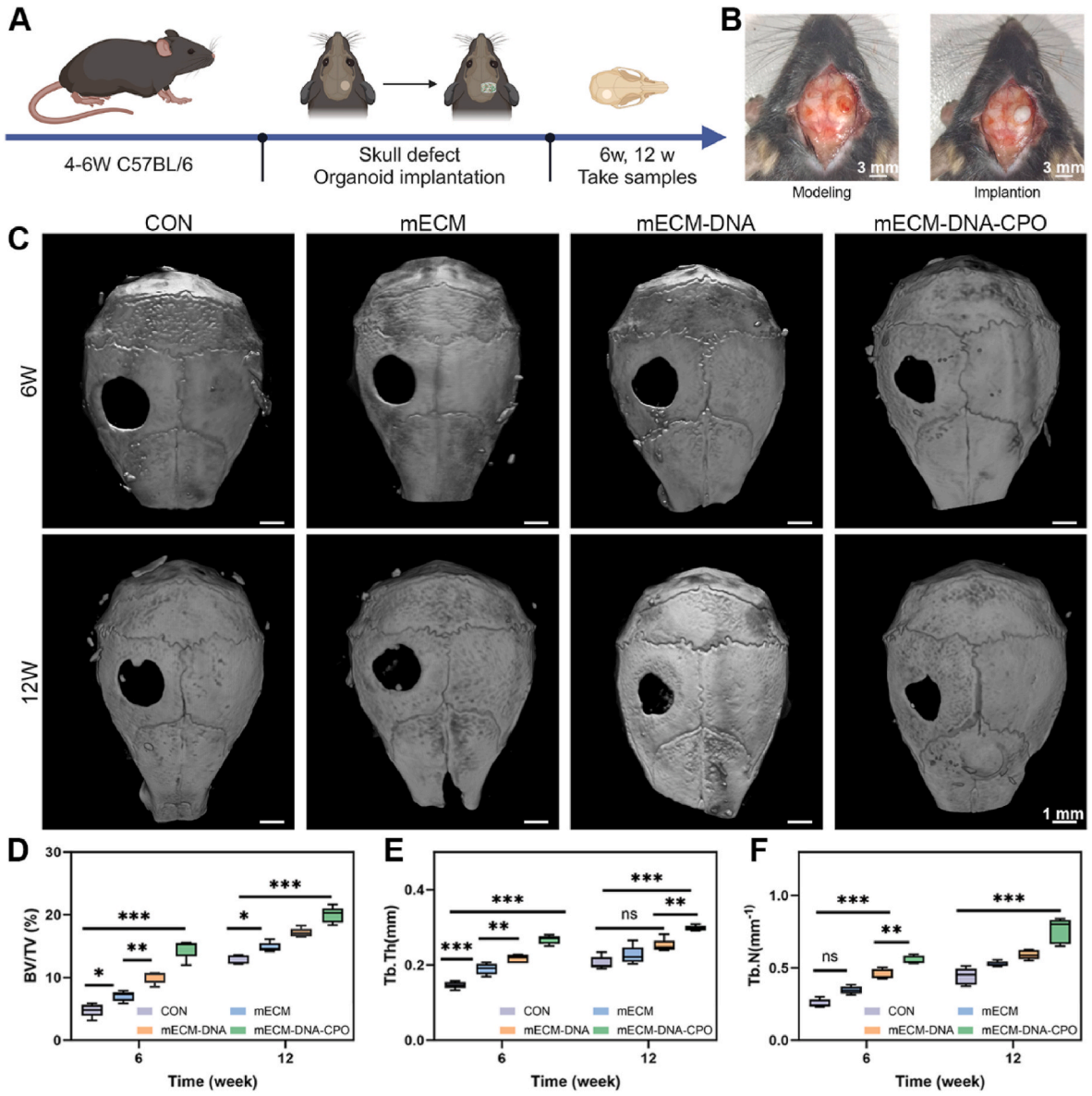

Fig. 9. Engineered bionic matrix hydrogels promote *in-situ* bone repair in cranial defect model. (A) Experimental workflow diagram for the mouse cranial defect model. (B) *In vivo* implantation of bone organoids. (C–F) Micro-CT reconstruction and analysis of mouse cranial samples at 6 and 12 weeks. All data were obtained from a minimum of n = 5 independent experiments and are expressed as mean ± SD. **P < 0.01, ***P < 0.001 compared to Blank group.

3.8. Bionic matrix hydrogels to construct vascularized bone organoids in vivo

We utilize the complex *in vivo* physiological microenvironment to construct vascularized bone organoids. This microenvironment provides essential biological signals for the development of vascularized bone organoids. Moreover, the rich and well-established vascular system *in vivo* supplies the necessary nutrients and oxygen for bone organoid construction, thereby accelerating the formation of vascularized bone organoids. Additionally, bone organoids constructed *in vivo* are more readily integrated with surrounding tissues, thereby speeding up the process of bone tissue repair. In the *in vivo* construction, we first assessed the degradation ability of the bionic matrix hydrogel (Fig. S10). We observed that after 5 weeks of implantation, the mECM-DNA group had completely degraded, while both the mECM and mECM-DNA-CPO groups still had some residual material. After 6 weeks of implantation, the mECM group still showed residual material, while the other two groups had completely degraded. This degradation trend is consistent with the results observed in the *in vivo* degradation study. Since bone tissue self-repair can be activated within one month, this bioinspired matrix hydrogel can activate the mineralization of bone organoids and promote bone tissue repair *in vivo*. Hydrogels loaded with BMSCs were subcutaneously implanted in nude mice and harvested after 2 and 4 weeks of culture to verify their ability to form bone organoids *in vivo* (Fig. 8A). Gross observation of the harvested *in vivo* bone organoids revealed that the organoids had become mostly transparent with noticeable white calcium deposition, with the mECM-DNA-CPO group showing the most prominent mineralization after 4 weeks. Furthermore, in the 2-week bone organoids, the mECM-DNA-CPO group exhibited a more distinct vascular network. While vascular networks were observed in all groups by 4 weeks, the mECM-DNA-CPO group showed a more prominent vascular network (Fig. 8B). Micro-CT analysis demonstrated that mineral deposition in the bone organoids significantly increased with extended *in vivo* culture time. Furthermore, at the same time point, the mECM-DNA-CPO group exhibited more prominent mineral deposition (Fig. 8C). The analysis of BMD and BV/TV also exhibited a similar trend, with these parameters significantly increased, consistent with the results from *in vivo* culture (Fig. 8D–E). Next, we conducted histological

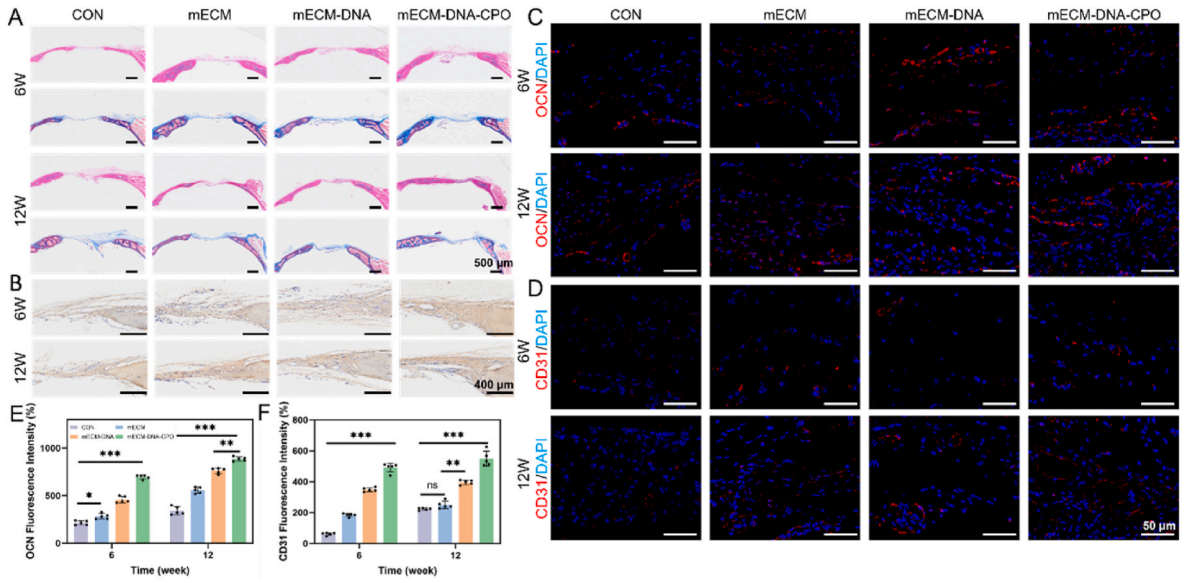

Fig. 10. Histological evaluation of *in situ* vascularized cranial bone repair. (A) HE and Masson staining. (B) Immunohistochemical staining of COL I. (C–D) OCN and CD31 immunofluorescence staining. (E–F) OCN and CD31 immunofluorescence quantitative analysis. All data were obtained from a minimum of n = 5 independent experiments and are expressed as mean ± SD. **P < 0.01, ***P < 0.001 compared to Blank group.

analysis of the *in vivo* organoids. Unlike *in vitro* culture, the majority of cells in the *in vivo* organoids were localized at the periphery of the vascularized bone organoids, with most of the central cells undergoing cell death. This phenomenon is likely due to the inability of the vasculature to supply nutrients to the central cells during the early stages of implantation, resulting in cell death. Immunofluorescence staining for CD31 revealed its expression in the bone organoids after 2 weeks of culture, though no tubular structures were observed at this stage. Immunohistochemical staining for COL I revealed distinct positive signals in the mECM-DNA-CPO group at 4 weeks post-implantation, demonstrating its superior osteogenic performance (Fig. 8F and S11A). By 4 weeks of culture, CD31 expression significantly increased, with well-defined tubular structures forming in both the mECM-DNA and mECM-DNA-CPO groups. Notably, the mECM-DNA-CPO group exhibited a prominent vascular network (Fig. 8G and S11B). These results demonstrate the superior performance of mECM-DNA-CPO in forming vascularized bone organoids *in vivo*, providing an excellent substrate for the construction of vascularized bone organoids and *in situ* vascularized bone repair.

3.9. Bionic matrix hydrogels promote in situ vascularized bone repair

Since mECM-DNA-CPO can form vascularized bone organoids through ectopic ossification, its implantation into cranial defect sites can achieve *in situ* vascularized bone repair by constructing vascularized bone organoids. To verify the effect of mECM-DNA-CPO on *in situ* vascularized repair of cranial bone defects, we created a 3 mm diameter cranial bone defect in mice and implanted mECM-DNA-CPO mixed with BMSCs into the defect site. Subsequently, animals were sacrificed at 6- and 12-weeks post-implantation, and three-dimensional reconstruction of the mouse calvarium was carried out using Micro-CT (Fig. 9A–B). Additionally, at 12 weeks post-surgery, H&E staining was conducted on the major organs of the mice, including the heart, liver, spleen, lungs, and kidneys. The results revealed no significant structural changes in these organs, confirming the excellent long-term biocompatibility of the bionic matrix hydrogel (Fig. S12). The Micro-CT reconstruction results demonstrated minimal new bone formation in the CON group at both 6- and 12-weeks post-surgery. In contrast, as the culture matrix was altered, the defect area gradually reduced, and the mECM-DNA-CPO group exhibited the smallest defect area at both time points (Fig. 9C). Subsequently, the bone repair capacity at the cranial defect site was assessed by measuring and analyzing BV/TV, trabecular thickness (Tb.Th), and trabecular number (Tb.N). As the culture matrix changed, all three values increased, indicating enhanced bone regenerative ability (Fig. 9D–F).

Additionally, H&E and Masson staining were carried out on cranial sections to evaluate new bone formation (Fig. 10A). Through staining, we observed that the CON group exhibited minimal new bone formation, with sparse tissue connections. In contrast, the treatment groups exhibited a progressive increase in new bone formation, with denser fibrous tissue and higher collagen content. Notably, the mECM-DNA-CPO group demonstrated the most pronounced osteogenic effect among all treatment groups. In addition, immunohistochemistry and immunofluorescence were utilized to evaluate osteogenesis-related markers (COL I and OCN). We found that, compared to the CON group, the treatment groups exhibited more pronounced positive results, with the mECM-DNA-CPO group showing the strongest positivity. This confirms that the bone organ constructed using mECM-DNA-CPO has a stronger osteogenic potential (Fig. 10B, C, E and S13). Furthermore, immunofluorescence analysis revealed a similar trend in the positive expression of the angiogenesis marker CD31. This further confirms that the bone organs constructed using mECM-DNA-CPO exhibit stronger angiogenic potential, promoting the synergistic regeneration of blood vessels and new bone (Fig. 10D–F).

4. Conclusion

In this study, we demonstrated that mineralized and vascularized bone organoids could be sequentially constructed using newly developed engineered bionic matrix hydrogels. These engineered ECM-DNA-CPO bionic matrix hydrogels exhibited excellent hydrophilicity, mechanical strength and viscoelastic properties, which well-mimicked bone conductive microenvironments with special inorganic/organic compositions and double-network dynamic structures. Interestingly, the engineered bionic matrix hydrogels effectively facilitated recruitment, proliferation, osteogenesis and angiogenesis of BMSCs, ultimately inducing the formation of mineralized and vascularized bone organoids via *in vitro* dynamic culture and *in vivo* heterotopic ossification. Furthermore, BMSCs-loaded engineered bionic matrix hydrogels showed remarkable efficacy in achieving *in-situ* bone regeneration in

cranial defect model. This study provide innovative strategies of engineered bone-mimicking matrix materials combined with such newly-developed dynamic culture system for addressing the unique requirements of functional bone organoids, advancing development and application of organoids in bone tissue regeneration.

CRediT authorship contribution statement

Tingting Gai: Writing – original draft, Methodology, Investigation, Formal analysis, Data curation, Conceptualization. **Hao Zhang:** Methodology, Investigation, Formal analysis. **Yan Hu:** Methodology, Investigation, Funding acquisition, Formal analysis. **Ruiyang Li:** Methodology, Investigation, Formal analysis. **Jian Wang:** Supervision, Software. **Xiao Chen:** Visualization, Validation, Supervision, Resources. **Jianhua Wang:** Validation, Software. **Zhenhua Chen:** Supervision, Resources. **Yingying Jing:** Visualization, Supervision, Resources. **Chenglong Wang:** Writing – review & editing, Supervision, Funding acquisition. **Long Bai:** Writing – review & editing, Supervision, Resources. **Xiuhui Wang:** Writing – review & editing, Supervision, Resources, Data curation, Conceptualization. **Jiacan Su:** Writing – review & editing, Supervision, Resources, Funding acquisition, Conceptualization.

Ethics approval and consent to participate

All animal experimental procedures were strictly conducted in accordance with the established guidelines for animal experiments and had received approval from the Animal Ethics Committee of Shanghai University (ECSHU-2024-122).

Declaration of competing interest

The authors declare the following personal relationships which may be considered as potential competing interests: Zhenhua Chen and Chenglong Wang are currently employed by Yantai Zhenghai Bio-tech Co., Ltd.

Acknowledgments

This work was supported by the National Natural Science Foundation of China (82230071, 82172098, 82472479, 82302397), Shanghai Committee of Science and Technology (23141900600).

Abbreviations

CPO: calcium phosphate oligomers; ECM: extracellular matrix; BMSCs: bone marrow mesenchymal stromal cells; HUVECs: human umbilical vein endothelial cells; LAP: Lithium Phenyl-2,4,6-trimethylbenzoylphosphinate; dECM: decellularized extracellular matrix; HAp: hydroxyapatite; DNA: deoxyribonucleic acid; mECM: methacrylated decellularized extracellular matrix; mECM-DNA: methacrylated decellularized extracellular matrix-deoxyribonucleic acid; mECM-DNA-CPO: methacrylated decellularized extracellular matrix-deoxyribonucleic acid-calcium phosphate oligomers; BMH: bionic matrix hydrogels; EDC: 1-(3-Dimethylaminopropyl)-3-ethylcarbodiimide; NHS: N-Hydroxysuccinimide; MA: methacrylic anhydride; MWCO: molecular weight cutoff; UV: ultraviolet; NMR: nuclear magnetic resonance; FTIR: Fourier transform infrared; EDS: energy dispersive spectroscopy; β-GP: β-glycerophosphate; mRNA-seq: Transcriptomic analysis.

Appendix A. Supplementary data

Supplementary data to this article can be found online at https://doi.org/10.1016/j.bioactmat.2025.02.033.

References

[1] X. Xue, Y. Hu, S. Wang, X. Chen, Y. Jiang, J. Su, Fabrication of physical and chemical crosslinked hydrogels for bone tissue engineering, Bioact. Mater. 12 (2022) 327–339.
[2] A. Salhotra, H.N. Shah, B. Levi, M.T. Longaker, Mechanisms of bone development and repair, Nat. Rev. Mol. Cell Biol. 21 (11) (2020) 696–711.
[3] J. Tuckermann, R.H. Adams, The endothelium-bone axis in development, homeostasis and bone and joint disease, Nat. Rev. Rheumatol. 17 (10) (2021) 608–620.
[4] X. Kong, T. Zheng, Z. Wang, T. Zhou, J. Shi, Y. Wang, B. Zhang, Remote actuation and on-demand activation of biomaterials pre-incorporated with physical cues for bone repair, Theranostics 14 (11) (2024) 4438–4461.
[5] M. Wang, F. Xia, Y. Wei, X. Wei, Molecular mechanisms and clinical management of cancer bone metastasis, Bone Res. 8 (1) (2020) 30.
[6] E.A. Masters, B.F. Ricciardi, K.L.d.M. Bentley, T.F. Moriarty, E.M. Schwarz, G. Muthukrishnan, Skeletal infections: microbial pathogenesis, immunity and clinical management, Nat. Rev. Microbiol. 20 (7) (2022) 385–400.
[7] X. Zhang, W. Jiang, C. Xie, X. Wu, Q. Ren, F. Wang, X. Shen, Y. Hong, H. Wu, Y. Liao, Y. Zhang, R. Liang, W. Sun, Y. Gu, T. Zhang, Y. Chen, W. Wei, S. Zhang, W. Zou, H. Ouyang, Msx1+ stem cells recruited by bioactive tissue engineering graft for bone regeneration, Nat. Commun. 13 (1) (2022) 5211.
[8] S. Li, L. Zhang, C. Liu, J. Kim, K. Su, T. Chen, L. Zhao, X. Lu, H. Zhang, Y. Cui, X. Cui, F. Yuan, H. Pan, Spontaneous immunomodulation and regulation of angiogenesis and osteogenesis by Sr/Cu-borosilicate glass (BSG) bone cement to repair critical bone defects, Bioact. Mater. 23 (2023) 101–117.
[9] R.J. Miron, Optimized bone grafting, Periodontol 94 (1) (2000) 143–160, 2024.
[10] C. Xie, J. Ye, R. Liang, X. Yao, X. Wu, Y. Koh, W. Wei, X. Zhang, H. Ouyang, Advanced strategies of biomimetic tissue-engineered grafts for bone regeneration, Adv. Healthcare Mater. 10 (14) (2021) e2100408.
[11] X. Xue, H. Zhang, H. Liu, S. Wang, J. Li, Q. Zhou, X. Chen, X. Ren, Y. Jing, Y. Deng, Z. Geng, X. Wang, J. Su, Rational design of multifunctional CuS nanoparticle-PEG composite soft hydrogel-coated 3D hard polycaprolactone scaffolds for efficient bone regeneration, Adv. Funct. Mater. 32 (33) (2022) e2202470.
[12] X. Yu, X. Tang, S.V. Gohil, C.T. Laurencin, Biomaterials for bone regenerative engineering, Adv. Healthcare Mater. 4 (9) (2015) 1268–1285.
[13] L. Bai, J. Su, Converging technologies in biomaterial translational research, Biomater. Transl. 4 (4) (2023) 197–198.
[14] D. Zhao, Q. Saiding, Y. Li, Y. Tang, W. Cui, Bone organoids: recent advances and future challenges, Adv. Healthcare Mater. 13 (5) (2024) e2302088.
[15] C. Shen, J. Wang, G. Li, S. Hao, Y. Wu, P. Song, Y. Han, M. Li, G. Wang, K. Xu, H. Zhang, X. Ren, Y. Jing, R. Yang, Z. Geng, J. Su, Boosting cartilage repair with silk fibroin-DNA hydrogel-based cartilage organoid precursor, Bioact. Mater. 35 (2024) 429–444.
[16] J. Huang, A. Li, R. Liang, X. Wu, S. Jia, J. Chen, Z. Jiao, C. Li, X. Zhang, J. Lin, Future perspectives: advances in bone/cartilage organoid technology and clinical potential, Biomater. Transl. 5 (4) (2024) 425–443.
[17] M.J. Shen, C.Y. Wang, D.X. Hao, J.X. Hao, Y.F. Zhu, X.X. Han, L. Tonggu, J. H. Chen, K. Jiao, F.R. Tay, L.N. Niu, Multifunctional nanomachinery for enhancement of bone healing, Adv. Mater. 34 (9) (2022) e2107924.
[18] S. Velasco, A.J. Kedaigle, S.K. Simmons, A. Nash, M. Rocha, G. Quadrato, B. Paulsen, L. Nguyen, X. Adiconis, A. Regev, J.Z. Levin, P. Arlotta, Individual brain organoids reproducibly form cell diversity of the human cerebral cortex, Nature 570 (7762) (2019) 523–527.
[19] A.J. Miller, B.R. Dye, D. Ferrer-Torres, D.R. Hill, A.W. Overeem, L.D. Shea, J. R. Spence, Generation of lung organoids from human pluripotent stem cells *in vitro*, Nat. Protoc. 14 (2) (2019) 518–540.
[20] L. Meran, L. Tullie, S. Eaton, P. De Coppi, V.S.W. Li, Bioengineering human intestinal mucosal grafts using patient-derived organoids, fibroblasts and scaffolds, Nat. Protoc. 18 (1) (2023) 108–135.
[21] X. Li, Z. Li, P. Wang, G. Lu, L. Tong, Q. Liu, Y. Chen, J. Lin, E. Luo, J. Liang, Q. Jiang, Y. Fan, X. Zhang, Y. Sun, Dopamine-integrated nanointerface between fibrillar matrix and hydrophilic nanohydroxyapatite regulates immune microenvironment to boost endogenous bone regeneration, Adv. Funct. Mater. 33 (16) (2023) e2212738.
[22] R. Nanda, S. Hazan, K. Sauer, V. Aladin, K. Keinan-Adamsky, B. Corzilius, R. Shahar, P. Zaslansky, G. Goobes, Molecular differences in collagen organization and in organic-inorganic interfacial structure of bones with and without osteocytes, Acta Biomater. 144 (2022) 195–209.
[23] S. Chen, X. Zhou, T. Li, C. He, Vascularization and innervation for bone tissue engineering, Acc. Mater. Res. 5 (9) (2024) 1121–1133.
[24] W. Hu, C. Wu, J. Long, Z. Zeng, Mechano-immunological checkpoints: an emerging strategy for investigation and evaluation of disease and therapeutics, Smart Materials in Medicine 5 (2) (2024) 256–260.
[25] K. Dai, Q. Zhang, S. Deng, Y. Yu, F. Zhu, S. Zhang, Y. Pan, D. Long, J. Wang, C. Liu, A BMP-2-triggered *in vivo* osteo-organoid for cell therapy, Sci. Adv. 9 (1) (2023) eadd1541.
[26] Z. Li, D. Yu, C. Zhou, F. Wang, K. Lu, Y. Liu, J. Xu, L. Xuan, X. Wang, Engineering vascularised organoid-on-a-chip: strategies, advances and future perspectives, Biomater. Transl. 5 (1) (2024) 21–32.
[27] Y. Zhao, Y. Cai, W. Wang, Y. Bai, M. Liu, Y. Wang, W. Niu, Z. Luo, L. Xia, J. Zhu, F. Zhao, F.R. Tay, L. Niu, Periosteum-bone inspired hierarchical scaffold with endogenous piezoelectricity for neuro-vascularized bone regeneration, Bioact. Mater. 44 (2025) 339–353.
[28] A. Akiva, J. Melke, S. Ansari, N. Liv, R. van der Meijden, M. van Erp, F. Zhao, M. Stout, W.H. Nijhuis, C. de Heus, C. Muñiz Ortera, J. Fermie, J. Klumperman,

K. Ito, N. Sommerdijk, S. Hofmann, An organoid for woven bone, Adv. Funct. Mater. 31 (17) (2021) e2010524.
[29] C. Xie, R. Liang, J. Ye, Z. Peng, H. Sun, Q. Zhu, X. Shen, Y. Hong, H. Wu, W. Sun, X. Yao, J. Li, S. Zhang, X. Zhang, H. Ouyang, High-efficient engineering of osteo-callus organoids for rapid bone regeneration within one month, Biomaterials 288 (2022) e121741.
[30] T. Gai, Y. Zhang, G. Li, F. Zhou, C. He, X. Wang, J. Su, Engineered hydrogel microspheres for spheroids and organoids construction, Chem. Eng. J. 498 (2024) e155131.
[31] C. Shen, Z. Zhou, R. Li, S. Yang, D. Zhou, F. Zhou, Z. Geng, J. Su, Silk fibroin-based hydrogels for cartilage organoids in osteoarthritis treatment, Theranostics 15 (2) (2025) 560–584.
[32] Q.Q. Wan, K. Jiao, Y.X. Ma, B. Gao, Z. Mu, Y.R. Wang, Y.H. Wang, L. Duan, K. H. Xu, J.T. Gu, J.F. Yan, J. Li, M.J. Shen, F.R. Tay, L.N. Niu, Smart, biomimetic periosteum created from the cerium (III, IV) oxide-mineralized eggshell membrane, ACS Appl. Mater. Interfaces 14 (12) (2022) 14103–14119.
[33] J. Hao, C. Qin, C. Wu, Three-dimensional multicellular biomaterial platforms for biomedical application, Interdisciplinary Materials 2 (5) (2023) 714–734.
[34] L. Zhu, J. Yuhan, H. Yu, B. Zhang, K. Huang, L. Zhu, Decellularized extracellular matrix for remodeling bioengineering organoid's microenvironment, Small 19 (25) (2023) e2207752.
[35] X. Zhang, X. Chen, H. Hong, R. Hu, J. Liu, C. Liu, Decellularized extracellular matrix scaffolds: recent trends and emerging strategies in tissue engineering, Bioact. Mater. 10 (2022) 15–31.
[36] S. Jiang, Y. Zhuang, M. Cai, X. Wang, K. Lin, Decellularized extracellular matrix: a promising strategy for skin repair and regeneration, Eng. Regen. 4 (4) (2023) 357–374.
[37] Q. Li, H. Yu, F. Zhao, C. Cao, T. Wu, Y. Fan, Y. Ao, X. Hu, 3D printing of microenvironment-specific bioinspired and exosome-reinforced hydrogel scaffolds for efficient cartilage and subchondral bone regeneration, Adv. Sci. 10 (26) (2023) e2303650.
[38] A. Tai, E. Landao-Bassonga, Z. Chen, M. Tran, B. Allan, R. Ruan, D. Calder, M. Goonewardene, H. Ngo, M.H. Zheng, Systematic evaluation of three porcine-derived collagen membranes for guided bone regeneration, Biomater. Transl 4 (1) (2023) 41–50.
[39] Y. Yu, Z. Guo, Y. Zhao, K. Kong, H. Pan, X. Xu, R. Tang, Z. Liu, A flexible and degradable hybrid mineral as a plastic substitute, Adv. Mater. 34 (9) (2022) e2107523.
[40] K. Liang, C. Zhao, C. Song, L. Zhao, P. Qiu, S. Wang, J. Zhu, Z. Gong, Z. Liu, R. Tang, X. Fang, Y. Zhao, *In situ* biomimetic mineralization of bone-like hydroxyapatite in hydrogel for the acceleration of bone regeneration, ACS Appl. Mater. Interfaces 15 (1) (2022) 292–308.
[41] Z. Liu, C. Shao, B. Jin, Z. Zhang, Y. Zhao, X. Xu, R. Tang, Crosslinking ionic oligomers as conformable precursors to calcium carbonate, Nature 574 (7778) (2019) 394–398.
[42] Y. Yu, K. Kong, R. Tang, Z. Liu, A bioinspired ultratough composite produced by integration of inorganic ionic oligomers within polymer networks, ACS Nano 16 (5) (2022) 7926–7936.
[43] G. Li, F. Gao, D. Yang, L. Lin, W. Yu, J. Tang, R. Yang, M. Jin, Y. Gu, P. Wang, E. Lu, ECM-mimicking composite hydrogel for accelerated vascularized bone regeneration, Bioact. Mater. 42 (2024) 241–256.
[44] Q. Yang, Y. Miao, J. Luo, Y. Chen, Y. Wang, Amyloid fibril and clay nanosheet dual-nanoengineered DNA dynamic hydrogel for vascularized bone regeneration, ACS Nano 17 (17) (2023) 17131–17147.
[45] D. Wang, J. Cui, M. Gan, Z. Xue, J. Wang, P. Liu, Y. Hu, Y. Pardo, S. Hamada, D. Yang, D. Luo, Transformation of biomass DNA into biodegradable materials from gels to plastics for reducing petrochemical consumption, J. Am. Chem. Soc. 142 (22) (2020) 10114–10124.
[46] A.K. Nair, A. Gautieri, S.-W. Chang, M.J. Buehler, Molecular mechanics of mineralized collagen fibrils in bone, Nat. Commun. 4 (2013) 1724.
[47] S. Hao, D. Zhou, F. Wang, G. Li, A. Deng, X. Ren, X. Wang, Y. Jing, Z. Shi, L. Bai, J. Su, Hamburger-like biomimetic nutrient periosteum with osteoimmunomodulation, angio-/osteo-genesis capacity promoted critical-size bone defect repair, Chem. Eng. J. 489 (2024) e150990.
[48] M. Liu, K. Liang, J. Zhen, M. Zhou, X. Wang, Z. Wang, X. Wei, Y. Zhang, Y. Sun, Z. Zhou, H. Su, C. Zhang, N. Li, C. Gao, J. Peng, F. Yi, Sirt6 deficiency exacerbates podocyte injury and proteinuria through targeting Notch signaling, Nat. Commun. 8 (1) (2017) 413.
[49] Y. Guo, X. Chi, Y. Wang, B.C. Heng, Y. Wei, X. Zhang, H. Zhao, Y. Yin, X. Deng, Mitochondria transfer enhances proliferation, migration, and osteogenic differentiation of bone marrow mesenchymal stem cell and promotes bone defect healing, Stem Cell Res. Ther. 11 (1) (2020) 245.
[50] R. Xiao, Q. Wang, J. Peng, Z. Yu, J. Zhang, Y. Xia, BMSC-derived exosomal Egr2 ameliorates ischemic stroke by directly upregulating SIRT6 to suppress Notch signaling, Mol. Neurobiol. 60 (1) (2023) 1–17.
[51] B. Jia, J. Chen, Q. Wang, X. Sun, J. Han, F. Guastaldi, S. Xiang, Q. Ye, Y. He, SIRT6 promotes osteogenic differentiation of adipose-derived mesenchymal stem cells through antagonizing DNMT1, Front. Cell Dev. Biol. 9 (2021) 648627.
[52] S.K. Ramasamy, A.P. Kusumbe, L. Wang, R.H. Adams, Endothelial Notch activity promotes angiogenesis and osteogenesis in bone, Nature 507 (7492) (2014) 376–380.